



1 **Soil related developments of the Biome-BGCMuSo v6.2**  
2 **terrestrial ecosystem model by integrating crop model**  
3 **components**

4

5 Dóra Hidy<sup>1,2\*</sup>, Zoltán Barcza<sup>1,3,4</sup>, Roland Hollós<sup>1,4</sup>, Laura Dobor<sup>5</sup>, Tamás Ács<sup>6</sup>, Dóra  
6 Zacháry<sup>7</sup>, Tibor Filep<sup>7</sup>, László Pásztor<sup>8</sup>, Dóra Incze<sup>3</sup>, Katarína Merganičová<sup>4,9</sup>, Peter  
7 Thornton<sup>10</sup>, Steven Running<sup>11</sup>, Nándor Fodor<sup>4</sup>

8

9 <sup>1</sup> Excellence Center, Faculty of Science, ELTE Eötvös Loránd University, H-2462 Martonvásár, Hungary

10 <sup>2</sup> Agroecology Research Group, MTA-MATE, H-2100 Gödöllő, Hungary

11 <sup>3</sup> Department of Meteorology, Institute of Geography and Earth Sciences, ELTE Eötvös Loránd University,  
12 H-1117 Budapest, Hungary

13 <sup>4</sup> Faculty of Forestry and Wood Sciences, Czech University of Life Sciences Prague, 165 21 Prague, Czech  
14 Republic

15 <sup>5</sup> Centre for Agricultural Research, Agricultural Institute, H-2462 Martonvásár, Hungary

16 <sup>6</sup> Department of Sanitary and Environmental Engineering, Budapest University of Technology and Economics,  
17 H-1111 Budapest, Hungary

18 <sup>7</sup> Geographical Institute, Research Centre for Astronomy and Earth Sciences, H-1112 Budapest, Hungary

19 <sup>8</sup> Institute for Soil Sciences, Centre for Agricultural Research, H-1022 Budapest, Hungary

20 <sup>9</sup> Department of Biodiversity of Ecosystems and Landscape, Institute of Landscape Ecology, Slovak Academy of  
21 Sciences, SK 949 01 Nitra, Slovakia

22 <sup>10</sup> Climate Change Science Institute/Environmental Sciences Division, Oak Ridge National Laboratory, Oak  
23 Ridge, TN 37831, USA

24 <sup>11</sup> Numerical Terradynamic Simulation Group, Department of Ecosystem and Conservation Sciences University  
25 of Montana, Missoula, MT 59812, USA

26

27 *Correspondence to:* Dora Hidy (dori.hidy@gmail.com)



28 **Abstract**

29 Terrestrial biogeochemical models are essential tools to quantify climate-carbon cycle  
30 feedback and plant-soil relations from local to global scale. In this study, theoretical basis is  
31 provided for the latest version of Biome-BGCMuSo biogeochemical model (version 6.2).  
32 Biome-BGCMuSo is a branch of the original Biome-BGC model with a large number of  
33 developments and structural changes. Earlier model versions performed poorly in terms of  
34 soil water content (SWC) dynamics in different environments. Moreover, lack of detailed  
35 nitrogen cycle representation was a major limitation of the model. Since problems associated  
36 with these internal drivers might influence the final results and parameter estimation,  
37 additional structural improvements were necessary. During the developments we took  
38 advantage of experiences from the crop modeller community where internal process  
39 representation has a long history. In this paper the improved soil hydrology and soil  
40 carbon/nitrogen cycle calculation methods are described in detail. Capabilities of the  
41 Biome-BGCMuSo v6.2 model are demonstrated via case studies focusing on soil hydrology  
42 and soil organic carbon content estimation. Soil hydrology related results are compared to  
43 observation data from an experimental lysimeter station. The results indicate improved  
44 performance for Biome-BGCMuSo v6.2 compared to v4.0 (explained variance increased from  
45 0.121 to 0.8 for SWC, and from 0.084 to 0.46 for soil evaporation; bias changed from -0.047  
46 to  $-0.007 \text{ m}^3 \text{ m}^{-3}$  for SWC, and from  $-0.68 \text{ mm day}^{-1}$  to  $-0.2 \text{ mm day}^{-1}$  for soil evaporation).  
47 Sensitivity analysis and optimization of the decomposition scheme is presented to support  
48 practical application of the model. The improved version of Biome-BGCMuSo has the ability  
49 to provide more realistic soil hydrology representation and nitrification/denitrification process  
50 estimation which represents a major milestone.

51

52



## 53 1. Introduction

54 The construction and development of biogeochemical models (BGM) is the response  
55 of the scientific community to address challenges related to climate change and human  
56 induced global environmental change. BGMs can be used to quantify future climate-  
57 vegetation interaction including climate-carbon cycle feedback, and as they simulate plant  
58 production, they can be used to study a variety of ecosystem services that are related to human  
59 nutrition and resource availability (Asseng et al., 2013; Bassu et al., 2014; Huntzinger et al.,  
60 2013). Similarly to the models describing various and complex environmental processes, the  
61 structure of biogeochemical models reflects our current knowledge about a complex system  
62 with many internal processes and interactions.

63 Processes of the atmosphere-plant-soil system take place on different temporal (sub-  
64 daily to centennial) scales and are driven by markedly different mechanisms that are  
65 quantified by a large diversity of modeling tools (Schwalm et al., 2019). Plant photosynthesis  
66 is an enzyme-driven biochemical process that has its own mathematical equation set and  
67 related parameters (and a large literature; e.g. Farquhar et al., 1980; Medlyn et al. 2002; Smith  
68 and Dukes, 2013; Dietze, 2013). Allocation of carbohydrates in the different plant  
69 compartments is studied extensively and also has a large literature and mathematical tool set  
70 (Friedlingstein et al., 1999; Olin et al., 2015; Merganičová et al., 2019). Plant phenology is  
71 quantified by specific algorithms that are rather uncertain components of the models  
72 (Richardson et al., 2013; Hufkens et al., 2018; Peaucelle et al., 2019). Soil biogeochemistry is  
73 driven by microbial and fungal activity and also has its own methodology and a vast literature  
74 (Zimmermann et al 2007; Kuzyakov, 2011; Koven et al., 2013; Berardi et al., 2020).  
75 Emerging scientific areas like the quantification of the dynamics of non-structural  
76 carbohydrates (NSC) in plants has a separate methodology that claims for mathematical  
77 representation in models (Martínez-Vilalta et al., 2016). Simulation of land surface hydrology  
78 including evapotranspiration is typically handled by some variant of the Penman-Monteith  
79 equation that is widely studied thus represents a separate scientific field (McMahon et al.,  
80 2013; Doležal et al., 2018).

81 Putting all together, if we are about to construct and further improve a biogeochemical  
82 model to consider novel findings and track global changes, we need a comprehensive  
83 knowledge that integrates many, almost disjunct scientific fields. Clearly, transparent and  
84 well-documented development of a biogeochemical model is of high priority but challenging



85 from the very beginning that claims for cooperation of researchers from various scientific  
86 fields.

87 Continuous model development is inevitable but it has to be supported by extensive  
88 comparison with observations and some kind of implementation of the model-data fusion  
89 approach (Keenan et al., 2011). It is well documented that structural problems might trigger  
90 incorrect parameter estimation that might be associated with distorted internal processes  
91 (Sándor et al., 2017; Martre et al., 2015). In other words, one major issue with BGMs (and in  
92 fact with all models using many parameters) is the possibility to get good simulation results  
93 for wrong reasons (which means incorrect parameterization) due to compensation of errors  
94 (Martre et al., 2015). In order to avoid this issue, any model developer team has to make an  
95 effort to focus also internal ecosystem conditions (e.g. soil volumetric water content (SWC),  
96 nutrient availability, stresses, etc.) and other processes (e.g. decomposition) rather than the  
97 main simulated processes (e.g. photosynthesis, evapotranspiration).

98 Historically, biogeochemical models have been developed to simulate the processes of  
99 undisturbed ecosystems with simple representation of the vegetation (Levis, 2010). As the  
100 focus was on the carbon cycle, water and nitrogen cycles and related soil processes were not  
101 well represented. Incorrect representation of SWC dynamics is still an issue with the models  
102 especially in drought-prone ecosystems (Sándor et al., 2017). Additionally, human  
103 intervention representation (management) was missing in many cases and it seems that some  
104 state-of-the-art BGMs still lack the representation of e.g. thinning, grass mowing, grazing,  
105 fertilization, planting or harvest (Table A1 in Friedlingstein et al., 2010).

106 In contrast, crop models with different complexity were used for about 50 years or so  
107 to simulate the processes of managed vegetation (Jones et al., 2017; Franke et al., 2020). As  
108 the focus of the crop models is on final yield due to economic reasons, the carbon balance, or  
109 the full greenhouse gas balance was not, or was just partially addressed originally. Crop  
110 models typically have a sophisticated representation of soil water balance with a multilayer  
111 soil module that usually calculates plant response to water stress as well. Nutrient stress, soil  
112 conditions during planting, consideration of multiple phenological phases, heat stress during  
113 anthesis, vernalization, manure application, fertilization, harvest, and many other processes  
114 have been implemented during the decades (Ewert et al., 2015). Therefore, it seems to be  
115 straightforward to exploit the benefits of crop models and implement sound and well-tested  
116 algorithms into the BGMs.

117 Our group has been developing Biome-BGCMuSo for 15 years. Starting from the  
118 well-known Biome-BGC model originally developed to simulate undisturbed forests and



119 grasslands, using a simple single layer soil submodel (Running and Hunt, 1993; Thornton and  
120 Rosenbloom, 2005), we developed a complex, more sophisticated model (Hidy et al., 2012;  
121 2016). Biome-BGCMuSo v4.0 (Biome-BGC with Multilayer Soil module) uses a 7-layer soil  
122 module and is capable of simulating different ecosystems from natural grassland to cropland  
123 including several management options, taking into account many environmental effects (Hidy  
124 et al., 2016). The developments included improvements regarding both soil and plant  
125 processes. In a nutshell, the most important, soil related developments were the improvement  
126 of the soil water balance module by implementing routines for estimating percolation,  
127 diffusion, pond water formation and runoff; the introduction of multilayer simulation for  
128 belowground processes in a simplified way. The most important, plant related developments  
129 involved the implementation of a routine for estimating the effect of drought on vegetation  
130 growth and senescence; the improvement of stomatal conductance calculation considering  
131 atmospheric CO<sub>2</sub> concentration; the integration of selected management modules; the  
132 implementation of new plant compartments (e.g. yield); the implementation of C4  
133 photosynthesis routine; the implementation of photosynthesis and respiration acclimation of  
134 plants and temperature-dependent Q10; and empirical estimation of methane and nitrous  
135 oxide soil efflux.

136 Problems found with the Biome-BGCMuSo v4.0 simulation result (such as the poor  
137 representation of soil water content (Hidy et al., 2016; Sándor et al., 2017) or the lack of  
138 sophisticated, layer-specific soil nitrogen dynamics representation) and the model structure  
139 related problems (such as the lubber parameterization of the model) marked the path for  
140 further developments.

141 The aim of the present study is to provide detailed documentation on the current,  
142 improved version of Biome-BGCMuSo v6.2, which has many new features and facilitates  
143 various in-depth investigations of ecosystem functioning. Due to large number of  
144 developments, this paper focuses only on the soil related model improvements. Case studies  
145 are also presented to demonstrate the capabilities of the new model version and to provide  
146 guidance for the model user community.

147

## 148 **2. The original Biome-BGC model**

149 Biome-BGC was developed from the Forest-BGC mechanistic model family in order  
150 to simulate vegetation types other than forests. Biome-BGC was one of the earliest



151 biogeochemical models that included explicit carbon and nitrogen cycle modules. Biome-  
152 BGC simulates the storages and fluxes of water, carbon, and nitrogen within and between the  
153 vegetation, litter, and soil components of terrestrial ecosystems. It uses a daily time step, and  
154 is driven by daily values of maximum and minimum temperatures, precipitation, solar  
155 radiation, and vapor pressure deficit (Running and Hunt, 1993). The model calculations apply  
156 to a unit ground area that is considered to be homogeneous.

157         The three most important components of the model are the phenological, the carbon  
158 uptake and release, and the soil flux modules. The core logic that is described below in this  
159 section remained intact during the developments. The phenological module calculates foliage  
160 development that affects the accumulation of C and N in leaf, stem (if present), root and  
161 consequently the amount of litter. In the carbon flux module gross primary production (GPP)  
162 of the biome is calculated using Farquhar's photosynthesis routine (Farquhar et al., 1980) and  
163 the enzyme kinetics model based on Woodrow and Berry (2003). Autotrophic respiration is  
164 separated into maintenance and growth respiration. Maintenance respiration is calculated as  
165 the function of the N content of living plant pools, while growth respiration is an adjustable  
166 but fixed proportion of the daily GPP. The single-layer soil module simulates the  
167 decomposition of dead plant material (litter) and soil organic matter, N mineralization and N  
168 balance in general (Running and Gower, 1991). The soil module uses the so-called  
169 converging cascade method (Thornton and Rosenbloom, 2005) to simulate decomposition,  
170 carbon and nitrogen turnover, and related soil CO<sub>2</sub> efflux.

171         The simulation has two basic steps. During the first (optional) spinup simulation the  
172 available climate data series is repeated as many times as it is required to reach a dynamic  
173 equilibrium in the soil organic matter content to estimate the initial values of the carbon and  
174 nitrogen pools. The second, normal simulation uses the results of the spinup simulation as  
175 initial conditions and runs for a given, predefined time period (Running and Gower 1991). So-  
176 called transient simulation option (which is the extension of the spinup routine) is a novel  
177 feature in Biome-BGCMuSo in order to ensure smooth transition between the spinup and  
178 normal phase (Hidy et al., 2021).

179         In Biome-BGC, the main parts of the simulated ecosystem are defined as plant, litter  
180 and soil. The most important pools include leaf (C, N and intercepted water), root (C, N),  
181 stem (C, N), soil (C, N and water) and litter (C, N). Plant C and N pools have sub-pools  
182 (actual pools, storage pools and transfer pools). The actual sub-pools store C and N for the  
183 current year growth. The storage sub-pools (essentially the non-structural carbohydrate pool,  
184 the source for the cores or buds) contain the amount of C and N that will be active during the



185 next growing season. The transfer sub-pools inherit the entire content of the storage pools at  
186 the end of every simulation year. Soil C also has sub-pools representing various organic  
187 matter forms characterized by considerably different decomposition rates.

188 In spite of its popularity and proven applicability, the development of Biome-BGC  
189 was temporarily stopped (the latest official NTSG version is Biome-BGC 4.2;  
190 <https://www.ntsg.umt.edu>). One major drawback of the model was its relatively poor  
191 performance in modelling managed ecosystems, and the simplistic soil water balance  
192 submodel using a single soil layer only.

193 Our team started to develop the Biome-BGC model further in 2006. According to the  
194 logic of the team, the new model branch was planned to be the continuation of the Biome-  
195 BGC model with regard to the original concept of the developers (keeping the model code  
196 open source, providing detailed documentation, and providing support for the users).

197 The starting point of our model development was Biome-BGC v4.1.1 that was a result  
198 of the model improvement activities of the Max Planck Institute (Vetter et al., 2007).  
199 Development of the Biome-BGCMuSo model branch has a long history by now. Previous  
200 model developments were documented in Hidy et al. (2012) and Hidy et al. (2016). Below,  
201 we provide detailed description of the new developments that are included in Biome-  
202 BGCMuSo v6.2 which is the latest version released in September, 2021. A comprehensive  
203 review of the input data requirement of the model together with explanation on the input data  
204 structure is available in the User's Guide (Hidy et al., 2021). In this paper we refer to some  
205 input files (e.g. soil file, plant file) that are described in the User's Guide in detail.

206 One of the most important novelty and advantage of the new model version (Biome-  
207 BGCMuSo v6.2) compared to any previous versions that due to the extensive and detailed  
208 soil parameter set (current version has 79, MuSo 4.0 has 39 and original model version has  
209 only 6 adjustable soil related parameters) the parameterization of the model is much more  
210 flexible. But this might be of course a challenging task to define all of the input parameters. In  
211 order to support practical application of the model, the User's Guide contains proposed values  
212 for most of the new parameters (Hidy et al., 2021).

### 213 **3. Soil hydrology related developments**

214 In Biome-BGCMuSo v6.2 a 10-layer soil submodel was implemented. Previous model  
215 versions included a 7-layer submodel, which turned out to be insufficient to capture  
216 hydrological events like drying of the topsoil layers with sufficient accuracy. The thicknesses



217 of the layers from the surface to the bottom are 3, 7, 20, 30, 30, 30, 30, 50, 200 and 600 cm.  
218 The centre of the given layer represents the depth of each soil layer. Soil texture can be  
219 defined by the percentage of sand and silt for each layer separately along with the most  
220 important physical and chemical parameters (pH, bulk density, characteristic SWC values,  
221 drainage coefficient, hydraulic conductivity) in the soil input file (Hidy et al., 2021).

222 The water balance module of Biome-BGCMuSo has five major components to  
223 describe soil water related processes in daily resolution (listed here following the order of  
224 calculation): pond water accumulation and runoff; infiltration and downward gravitational  
225 flow (percolation); water potential gradient driven water movement within the soil (diffusion);  
226 evaporation and transpiration (root water uptake); and the downward/upward fluxes to/from  
227 groundwater. In the following subsections these five major components are described.

### 228 **3.1 Pond water accumulation and runoff**

229 Precipitation can reach the surface as rain or snow (below 0 °C snow accumulation is  
230 assumed). Snow water melts from the snowpack as a function of temperature and radiation  
231 and added to the precipitation input.

232 The canopy can intercept rain. The intercepted volume goes into the *canopy water*  
233 pool, which can evaporate. No canopy interception of snow is assumed. The throughfall  
234 (complemented with the amount of melted snow) gives the potential infiltration.

235 Important novelty of Biome-BGCMuSo v6.2 is that maximum infiltration is calculated  
236 based on the saturated hydraulic conductivity and the SWC of the top soil layers. If the  
237 potential infiltration exceeds the maximum infiltration, pond water can be formed. If the sum  
238 of the precipitation and the actual pond height minus the maximum infiltration rate is greater  
239 than the maximum pond height, the excess water is added to surface runoff detailed below  
240 (Balsamo et al., 2009). The maximum pond height is an input parameter. Water from the pond  
241 can infiltrate into the soil at a rate the top soil layer can absorb it. Evaporation of the pond  
242 water is assumed equal to the potential evaporation.

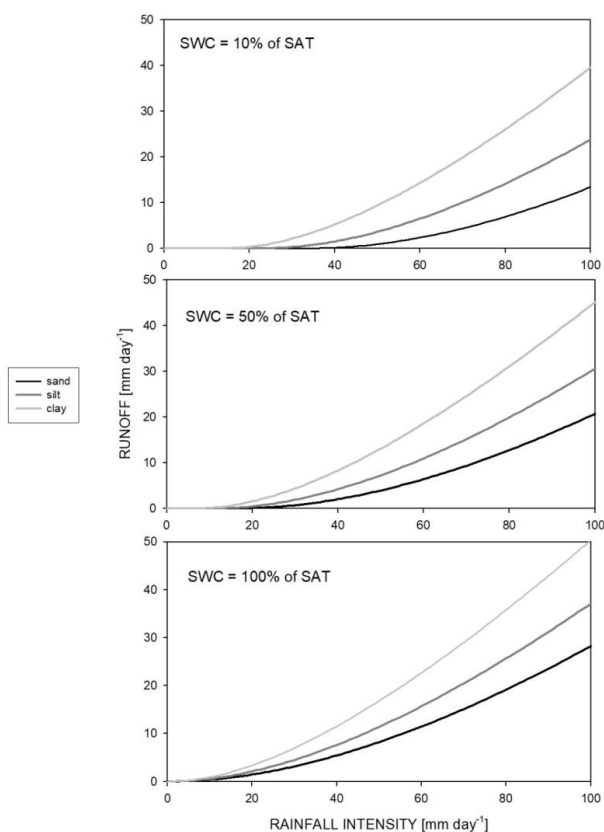
243 Surface runoff is the water flow occurring on the surface when a portion of the  
244 precipitation cannot infiltrate into the soil. Two types of surface runoff processes can be  
245 distinguished: Hortonian and Dunne. Hortonian runoff is unsaturated overland flow that  
246 occurs when the rate of precipitation exceeds the rate at which water can infiltrate. The other  
247 type of surface runoff is the Dunne runoff (also known as the saturation overland flow) which  
248 occurs when the entire soil is saturated but the rain continues to fall. In this case the rainfall  
249 immediately triggers pond water formation and (above the maximum pond water height)





250 surface runoff. The handling of these processes is presented in the soil hydrological module of  
251 Biome-BGCMuSo v6.2.

252 Calculation of Hortonian runoff (in  $\text{kg H}_2\text{O m}^{-2} \text{ day}^{-1}$ ) is based on a semi-empirical  
253 method and uses the precipitation amount (in  $\text{cm day}^{-1}$ ), the unitless runoff curve number  
254 ( $RCN$ ), and the actual moisture content status of the topsoil (Rawls et al., 1980; this method is  
255 known as the SCS runoff curve number method). This type of runoff simulation can be turned  
256 off by setting  $RCN$  to zero. The detailed description can be found in the Supplementary  
257 material, Section 1. The amount of runoff as a function of the soil type and the actual SWC is  
258 presented in Figure 1.



259  
260 **Figure 1: Hortonian runoff as the function of rainfall intensity, soil type and actual soil water content of the top soil**  
261 **layer. Sand soil means 92% sand, 4% silt and 4% clay; silt soil means 8% sand, 86% silt and 6% clay; clay soil means**  
262 **20% sand, 20% silt and 60% clay. SWC means soil water content; SAT means saturation.**

263



## 264 3.2 Infiltration, percolation and diffusion

265 There are two optional methods in Biome-BGCMuSo v6.2 to calculate soil water  
266 movement between soil layers and actual SWC layer by layer. The first one is a cascade  
267 method (also known as tipping bucket method), and the second is a Richards equation based  
268 physical method. The tipping bucket method has a long history in crop modelling and is  
269 considered as a successful, well-evaluated algorithm that can accurately simulate downward  
270 water flow in the soil.

271 The cascade method uses a semi-empirical input parameter ( $DC$ : drainage coefficient  
272 in  $\text{day}^{-1}$ ) to calculate downward water flow rate. When the SWC of a soil layer exceeds field  
273 capacity (FC), a fraction (equal to  $DC$ ) of the water amount above FC goes to the layer next  
274 below. If  $DC$  is not set in the soil input file, it is estimated from the saturated hydraulic  
275 conductivity:  $DC = 0.1122 \cdot K_{SAT}^{0.339}$  ( $K_{SAT}$ : saturated hydraulic conductivity in  $\text{cm day}^{-1}$ ;  
276 the user can set its value or the model based on soil texture estimates it internally; see Hidy et  
277 al., 2016). The detailed description of the method can be found in the Supplementary material,  
278 Section 2. Drainage from the bottom layer is a net loss for the soil profile.

279 Water diffusion that is the capillary water flow between the soil layers is calculated to  
280 account for the relatively slow movement of water. The flow rate is the function of the water  
281 content difference of two adjacent layers and the soil water diffusivity at the boundary of the  
282 layers, which is determined based on the average water content of the two layers. The detailed  
283 mathematical description of the method can be found in the Supplementary material, Section  
284 3.

285 The detailed description of the Richards method can be found in Hidy et al. (2012). To  
286 support efficient and robust calculations of soil water fluxes a dynamically changing time step  
287 was introduced in version 4.0 (Hidy et al., 2016). An enhancement of this method in Biome-  
288 BGCMuSo v6.2 is the finer vertical discretisation of the soil profile that is used during the  
289 numerical solution of the equation. The implementation of the Richards-equation is still in an  
290 experimental phase requiring rigorous testing and validation in the future.

## 291 3.3 Evapotranspiration

292 Biome-BGCMuSo, such as its predecessor Biome-BGC, estimates evaporation of leaf  
293 intercepted water, bare soil evaporation, and transpiration to estimate the total  
294 evapotranspiration in a daily level. The potential rates of all three processes are calculated  
295 based on the Penman-Monteith (PM) method. PM equation requires net radiation (minus soil



296 heat flux) and conductance values by definition using different parameterization for the  
297 different processes. The model calculates leaf- and canopy-level conductances of water  
298 vapour and sensible heat fluxes, to be used in Penman-Monteith calculations of canopy  
299 evaporation and canopy transpiration. Note that in the Biome-BGC model family the direct  
300 wind effect is ignored but can be considered indirectly by adjusting boundary layer  
301 conductance to site-specific conditions. A possible future direction might be the extension of  
302 the model logic to consider wind effect directly.

### 303 3.3.1 Canopy evaporation

304 If there is intercepted water, this portion of evaporation is calculated using the canopy  
305 resistance (reciprocal of conductance) to evaporated water and the resistance to sensible heat.  
306 The time required for the water to evaporate based on the average daily conditions is  
307 calculated, and subtracted from the day length to get the effective day length for  
308 evapotranspiration. Combined resistance to convective and radiative heat transfer is calculated  
309 based on canopy conductance of vapour and leaf conductance of sensible heat both of which  
310 are assumed to be equal to the boundary layer conductance. Besides the  
311 conductance/resistance parameters the canopy absorbed shortwave radiation drives the  
312 calculation. Note that the canopy evaporation routine was not modified significantly in  
313 Biome-BGCMuSo.

### 314 3.3.2 Soil evaporation

315 In order to estimate soil evaporation, first the potential evaporation is calculated,  
316 assuming that the resistance to vapour is equal to the resistance to sensible heat and assuming  
317 no additional resistance component. Both resistances are assumed to be equal to the actual  
318 aerodynamic resistance. Actual aerodynamic resistance is the function of the actual air  
319 pressure and air temperature and the potential aerodynamic resistance ( $potR_{air}$  in  $s\ m^{-1}$ ).  
320  $potR_{air}$  was a fixed value in the previous model versions ( $107\ s\ m^{-1}$ ). Its value was derived  
321 from observations over bare soil in tiger-bush in south-west Niger (Wallace and Holwill,  
322 1997). In Biome-BGCMuSo v6.2, the  $potR_{air}$  is an input parameter that can be adjusted by the  
323 user (Hidy et al., 2021). Another new development in Biome-BGCMuSo v6.2 is the  
324 introduction of an upper limit for daily potential evaporation ( $evap_{limit}$ ) that is determined by  
325 the available energy (incident shortwave flux that reaches the soil surface):

$$326\ evap_{limit} = \frac{irad \cdot dayl}{LH_{vap}} \quad (1)$$



327 where  $irad$  is the incident shortwave flux density in  $W m^{-2}$ ,  $dayl$  is the length of the day in  
328 seconds,  $LH_{vap}$  is the latent heat of vaporization (the amount of energy that must be added to  
329 liquid to transform into gas) in  $J kg^{-1}$ . This feature was missing from previous model versions  
330 resulting in considerable overestimation of evaporation on certain days that was caused by the  
331 missing energy limitation on evaporation.

332 An important novelty in Biome-BGCMuSo v6.2 is the calculation of the actual  
333 evaporation from the potential evaporation and the square root of time elapsed since the last  
334 precipitation (expressed by days; Ritchie, 1998). This is another method that has been used by  
335 the crop modeller community for many years. Detailed description of the algorithm can be  
336 found in the Supplementary material, Section 4.

337 A major novel feature in Biome-BGCMuSo v6.2 is the simulation of the reducing  
338 effect of surface residue or mulch cover on bare soil evaporation. Here we use the term  
339 ‘mulch’ to quantify surface residue cover in general keeping in mind that mulch is typically a  
340 human-induced coverage. Surface residue includes aboveground litter and coarse woody  
341 debris as well.

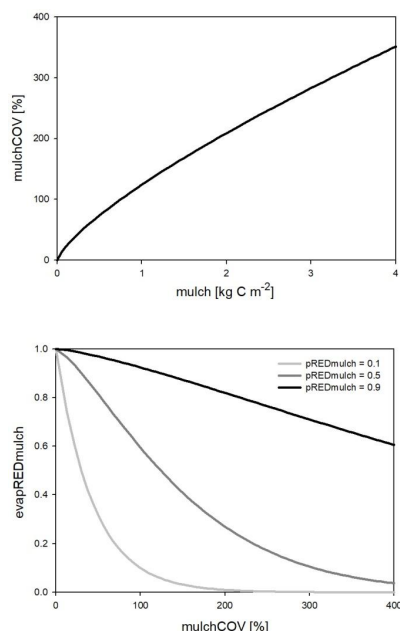
342 The evaporation reduction effect ( $evapREDmulch$ ; unitless) is a variable between 0  
343 and 1 (0 means full limitation, and 1 means no limitation) estimated based on a power  
344 function of the surface coverage ( $mulchCOV$  in %) and a soil specific constant set by the user  
345 ( $pREDmulch$ ; see Hidy et al., 2021). If variable  $mulchCOV$  reaches 100% it means that the  
346 surface is completely covered. If  $mulchCOV$  is greater than 100% it means the surface is  
347 covered by more than one layers. Surface coverage is a power function of the amount of  
348 mulch ( $mu$  in  $kgC m^{-2}$ ) with parameters  $p1_{mulch}$ ,  $p2_{mulch}$ , and  $p3_{mulch}$  (soil parameters) based  
349 on the method of Rawls et al. (1991):

350

$$351 \quad mulchCOV = p1_{mulch} \cdot (mu/p2_{mulch})^{p3_{mulch}} \quad (2)$$

$$352 \quad evapREDmulch = pREDmulch \frac{mulchCOV}{100} \quad (3)$$

353 Another simulated effect of surface residue cover is the homogenization of soil  
354 temperature between 0 and 30 cm depth (layers 1, 2 and 3). The functional forms of surface  
355 coverage and evaporation reduction factor are presented in Figure 2.



356

357 **Figure 2: Surface coverage as a function of the amount of surface residue or mulch (upper plot) and the evaporation**  
358 **reduction factor (evapREDmulch) as the function of mulch coverage (lower plot) using different mulch specific soil**  
359 **parameters (pREDmulch). See text for details.**

360

### 361 3.3.3 Transpiration

362 In order to simulate transpiration, first transpiration demand ( $TD$  in  $\text{kg H}_2\text{O m}^{-2} \text{ day}^{-1}$ )  
363 is calculated using the Penman-Monteith equation separately for sunlit and shaded leaves.  $TD$   
364 is the function of leaf-scale conductance to water vapor, which is derived from stomatal,  
365 cuticular and leaf boundary layer conductances. A novelty in Biome-BGCMuSo v6.2 is that  
366 potential evapotranspiration is also calculated using the maximal stomatal conductance  
367 instead of the actual stomatal conductance, which means that stomatal aperture is not affected  
368 by the soil moisture status (in contrast to the actual one).

369  $TD$  is distributed across the soil layers according to the actual root distribution using  
370 an improved method (the logic was changed since Biome-BGCMuSo v4.0). From the plant  
371 specific root parameters and the actual root weight Biome-BGCMuSo calculates the number  
372 of the layers where roots can be found together with the root mass distribution across the  
373 layers. If there is not enough water in a given soil layer to fulfil the transpiration demand, the  
374 transpiration flux from that layer is limited, and below wilting point (WP) it is set to zero. The  
375 sum of layer-specific transpiration fluxes across the root zone gives the actual transpiration



376 flux. The detailed description of the algorithm can be found in the Supplementary material,  
377 Section 5.

### 378 **3.4 Effect of groundwater**

379 Simulation of groundwater effect was introduced in Biome-BGCMuSo v4.0 (Hidy et  
380 al., 2016), but the method has been significantly improved, and the new algorithm it is now  
381 available in Biome-BGCMuSo v6.2. In the recent model version there is an option to provide  
382 an additional input file with the daily values of the groundwater table depth (*GWdepth* in m).

383 Groundwater may affect soil hydrological and plant physiological processes if the  
384 water table is closer to the root zone than the thickness of the capillary fringe (that is the  
385 region saturated from groundwater via capillary effect). The thickness of the capillary fringe  
386 (*CF* in m) is estimated using literature data and depends on the soil type (Johnson and Ettinger  
387 model; Tillman and Weaver, 2006). Groundwater table distance (*GWdist* in m) for a given  
388 layer is defined as the difference between *GWdepth* and the depth of the midpoint of the  
389 layer.

390 The layers completely below the groundwater table are assumed to be fully saturated.  
391 In case of layers within the capillary fringe ( $GWdist < CF$ ), the calculation of water balance  
392 changes: the field capacity rises, thus the difference between saturation (SAT) and FC  
393 decreases and the layer charges gradually, till the increased FC value is reached. The FC-  
394 rising effect of groundwater for the layers above the water table is calculated based on the  
395 ratio of the groundwater distance and the capillary fringe thickness, but only after the water  
396 content of the layers below have reached their modified FC values. Detailed description of the  
397 groundwater effect can be found in Supplementary material, Section 6.

### 398 **3.5 Soil moisture stress**

399 In the original Biome-BGC model the effect of changing soil water content on  
400 photosynthesis and decomposition of soil organic matter is expressed in terms of soil water  
401 potential ( $\Psi$ ). Instead of  $\Psi$ , the volumetric SWC is also widely used to calculate the limitation  
402 of stomatal conductance and decomposition. A practical advantage of using SWC as a factor  
403 in stress function is that it is easier to measure in the field and the changes of the driving  
404 function are much smoother than in case of  $\Psi$ . The disadvantage is that SWC is not  
405 comparable among different soil types (in contrast to  $\Psi$ ).



406 The maximum of SWC is the saturation value; the minimum is the wilting point or the  
 407 hygroscopic water depending on the type of the simulated process. Novelty of Biome-  
 408 BGCMuSo v6.2 is that the hygroscopic water, the wilting point, the field capacity and the  
 409 saturation values are calculated internally by the model based on the soil texture data, or can  
 410 be defined in the input file layer by layer.

411 In Biome-BGCMuSo v6.2 the so-called soil moisture stress index (*SMSI*) is calculated  
 412 to represent overall soil stress conditions. *SMSI* is affected by the length of the drought event  
 413 (*SMSE*: extent of soil stress), the severity of the drought event (*SMSL*: length of soil stress),  
 414 aggravated by the extreme temperature (*extremT*: effect of extreme heat). *SMSI* is equal to  
 415 zero if no soil moisture limitation occurs and equal to 1 in case of full soil moisture limitation.  
 416 *SMSI* is used by the model for plant senescence calculations (presentation of plant related  
 417 processes is the subject of a forthcoming publication)). The members of *SMSI* are explained  
 418 detailed below.

419

$$420 \quad SMSI = 1 - SMSE \cdot SMSL \cdot extremT \quad (4)$$

421 Magnitude of soil moisture stress (*SMSE*) is calculated layer by layer based on SWC.  
 422 Regarding soil moisture stress two different processes are distinguished: drought (i.e. low  
 423 SWC close to or below WP) and anoxic condition (i.e. after large precipitation events or in  
 424 the presence of high groundwater table; Bond-Lamberty et al., 2007). An important novelty of  
 425 Biome-BGCMuSo v6.2 is the soil curvature parameters (*q*) which is introduced to provide  
 426 mechanism for soil texture dependent drought stress as it can affect the shape of the soil stress  
 427 function (which means possibility for non-linear ramp function):

428

$$429 \quad SMSE^i = 0 \quad ; SWC^i < SWC_{WP}^i$$

$$430 \quad SMSE^i = \left( \frac{SWC^i - SWC_{WP}^i}{SWC_{drought}^i - SWC_{WP}^i} \right)^q \quad ; SWC_{WP}^i \leq SWC < SWC_{drought}^i \quad (5)$$

$$431 \quad SMSE^i = 1 \quad ; SWC_{drought}^i \leq SWC \leq SWC_{anoxic}^i$$

$$432 \quad SMSE^i = \frac{SWC_{SAT}^i - SWC^i}{SWC_{SAT}^i - SWC_{anoxic}^i} \quad ; SWC^i > SWC_{anoxic}^i$$

433 where *q* is the curvature of soil stress function,  $SWC_{drought}^i$  and  $SWC_{anoxic}^i$  are critical SWC  
 434 values for calculating soil stress.

435 In order to make the SWC values comparable between different soil types,  
 436  $SWC_{drought}^i$  and  $SWC_{anoxic}^i$  can be set in normalized form (such as in Eq. 4) as part of the



437 ecophysiological parameterization of the model. More details about the adjustment of the  
438 critical SWC values can be found in Hidy et al. (2021).

439 The layer specific soil moisture stress extent values are summed across the root zone  
440 using the relative amount of roots in the layers ( $RP^i$ ) as weighting factors to obtain the overall  
441 soil moisture stress extent ( $SMSE$ ):

$$442 \quad SMSE = \sum_{i=0}^{i=nr} SMSE^i \cdot RP^i \quad (6)$$

$$443 \quad RP^i = RD \frac{z^i}{RL} \cdot e^{-RD \cdot (mid^i / RL)} \quad (7)$$

444 where  $nr$  is the number of the soil layers where roots can be found,  $RL$  is the actual length of  
445 roots,  $RD$  is rooting distribution parameter (ecophysiological parameter; see details in the  
446 User's Guide; Hidy et al., 2021). In the current model version  $SMSE$  can also affect the entire  
447 photosynthetic machinery by the introduction of an empirical parameter. This mechanism is  
448 responsible to account for the non-stomatal effect of drought on photosynthesis (details about  
449 this algorithm will be published in a separate paper). Since there is no mechanistic  
450 representation behind this empirical down-regulation of photosynthesis, further test are  
451 needed for the correct setting of this parameter using preferentially eddy covariance data.

452 The soil moisture stress length related factor ( $SMSL$ ) is the ratio of the critical soil  
453 moisture stress length (ecophysiological parameter) and the sum of the daily ( $1 - SMSE$ )  
454 values. This cumulated value restarts if  $SMSE$  is equal to one (no stress). Extreme heat  
455 ( $extremT$ ) is also considered and is taken into account in the final stress function (see above)  
456 by using a ramp function. Its parameterization thus requires the setting of two critical  
457 temperature limits that defines the ramp function (set by the ecophysiological  
458 parameterization; see Hidy et al., 2021). Its characteristic temperature values can be set by  
459 parameterization (ecophysiological input file).

## 460 **4. Soil carbon and nitrogen cycles**

### 461 **4.1 Soil-litter module**

462 We made substantial changes in the soil biogeochemistry module of the Biome-BGC  
463 model. Previous model versions already offered solutions for multilayer simulations (Hidy et  
464 al., 2012, 2016), but some pools still inherited the single-layer logic of the original model. In  
465 the new model version all relevant soil processes are separated layer by layer which is a major  
466 step forward.



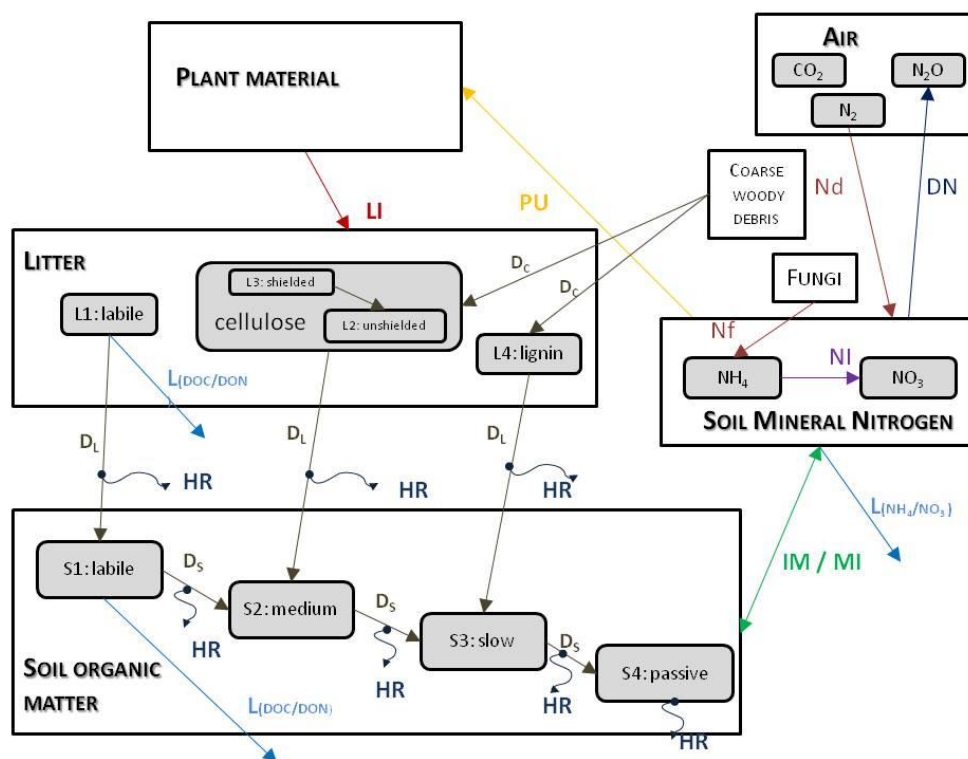


467            Instead of defining a single litter, soil organic carbon (SOC) and nitrogen pool, we  
468 implemented separate carbon and nitrogen pools for each soil layer in the form of soil organic  
469 matter (SOM) and litter in Biome-BGCMuSo v6.2. The changes of the mass of the carbon and  
470 nitrogen pools are calculated layer by layer. Mortality fluxes (whole plant mortality,  
471 senescence, litterfall) of aboveground plant material are transferred into the litter pools of the  
472 top soil layers (0-10 cm, layers 1-2). Mortality fluxes of belowground plant material are  
473 transferred into the corresponding soil layers based on their location within the root zone. Due  
474 to ploughing and leaching, carbon and nitrogen can also be relocated to deeper layers. The  
475 plant material turning into the litter compartment is divided between the different types of  
476 litter pools (labile, unshielded cellulose, shielded cellulose and lignin) according to the  
477 parameterization. Litter and soil decomposition fluxes (carbon and nitrogen fluxes from litter  
478 to soil pools) are calculated layer by layer, depending on the actual temperature and SWC of  
479 the corresponding layers. Vertical mixing of soil organic matter between the soil layers (e.g.  
480 bioturbation) is not implemented in the current model version.

481            Figure 3 shows the most important simulated soil and litter processes. N-fixation ( $Nf$ )  
482 is the N input from the atmosphere to soil layers in the root zone by microorganisms. The user  
483 can set its annual value as an input parameter. N-deposition ( $Nd$ ) is the N input from the  
484 atmosphere to the top soil layers (see below). The user can set its annual value as a site-  
485 specific parameter in the initialization input file. Nitrogen deposition can be provided by  
486 annually varying values as well. Plant uptake ( $PU$ ) is the absorption of mineral N by plants  
487 from the soil layers in the root zone. Mineralization ( $M$ ) is the release of plant-available  
488 nitrogen (flux from soil organic matter to mineralized nitrogen). Immobilization ( $IM$ ) is the  
489 consumption of inorganic nitrogen by microorganisms (flux from mineralized nitrogen to soil  
490 organic matter). Nitrification ( $N$ ) is the biological oxidation of ammonium to nitrate through  
491 nitrifying bacteria. Denitrification ( $DN$ ) is a microbial process where nitrate ( $\text{NO}_3^-$ ) is reduced  
492 and converted to nitrogen gas ( $\text{N}_2$ ) through intermediate nitrogen oxide gases. Leaching ( $L$ )  
493 is the loss of water-soluble mineral nitrogen from the soil layers. If leaching occurs in the  
494 lowermost soil layer that means loss of N from the simulated system. Litterfall ( $Ll$ ) is the  
495 plant material transfer from plant compartments to litter. Decomposition is the C and N  
496 transfer from litter to soil pools and between soil pools. In case of woody vegetation coarse  
497 woody debris (CWD) contains the woody plant material after litterfall before physical  
498 fragmentation. Litter has also four sub-pools based on their composition: labile (L1),  
499 unshielded and shielded cellulose (L2, L3) and lignin (L4). Soil organic matter has also four



500 sub-pools based on their turnover rate: labile (S1), medium (S2), slow (S3) and passive  
 501 (recalcitrant; S4) SOM pool. Soil mineralized nitrogen pool contains the inorganic N-forms of  
 502 the soil: ammonium and nitrate.



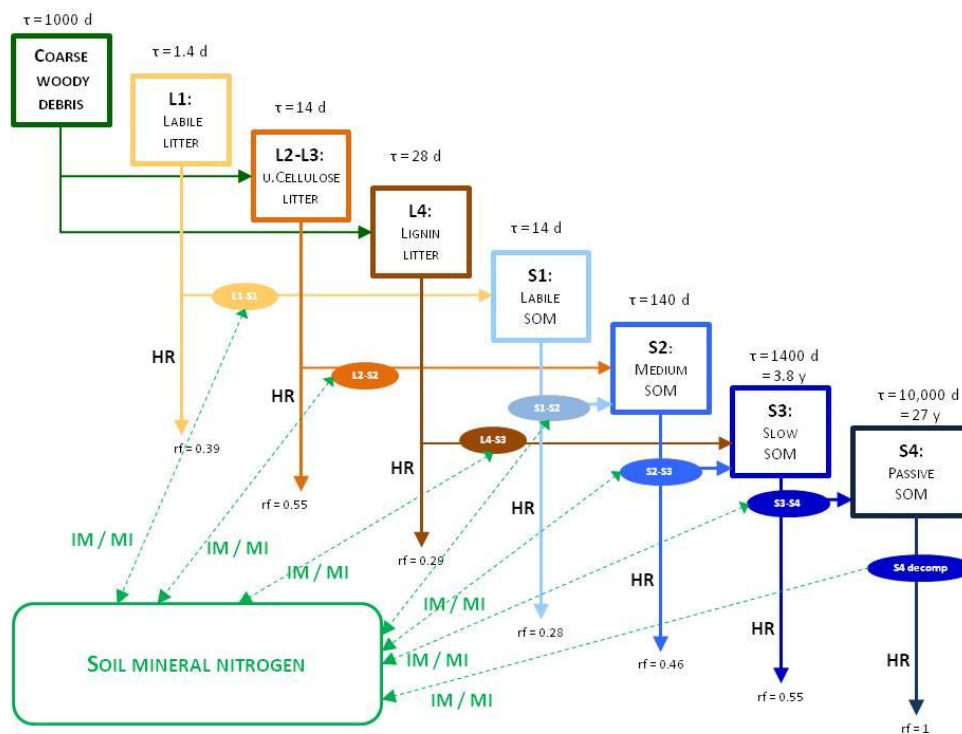
503  
 504 **Figure 3: Soil and litter related simulated carbon/nitrogen fluxes (arrows) and pools (rectangles) in Biome-BGCMuSo**  
 505 **v6.2. HR: heterotrophic respiration, IM: immobilization, MI: mineralization, PU: plant uptake, LI: litterfall, NI:**  
 506 **nitrification, D: decomposition ( $D_L$ : decomposition of litter,  $D_s$ : decomposition of SOM,  $D_C$ : fragmentation of coarse**  
 507 **woody debris), L: leaching,  $N_f$ : nitrogen fixation,  $N_d$ : nitrogen deposition,  $DN$ : denitrification. L represents loss of C**  
 508 **and N from the simulated system.**

509

## 510 4.2 Decomposition

511 In the decomposition module (i.e. converging cascade scheme; Thornton, 1998) the  
 512 fluxes between litter and soil pools are calculated layer by layer. The potential fluxes are  
 513 modified in case of N limitation when the potential gross immobilization is greater than the  
 514 potential gross mineralization.

515 To explain the decomposition processes implemented in Biome-BGCMuSo v6.2 the  
 516 main carbon/nitrogen pools and fluxes between litter and soil organic and inorganic  
 517 (mineralized) matter are presented on Figure 4.



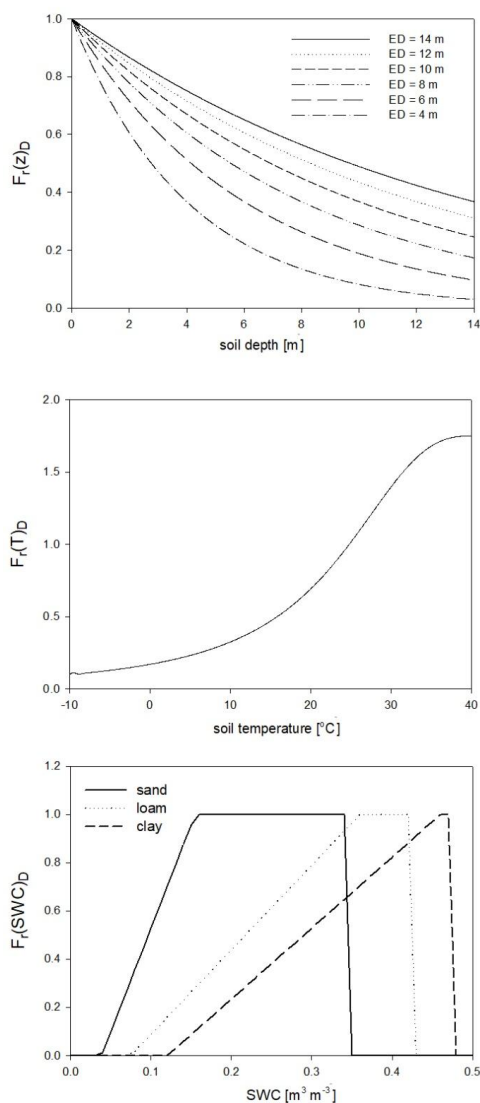
518

519 **Figure 4: Overview of the converging cascade model of litter and soil organic matter decomposition that is**  
 520 **implemented in Biome-BGCMuSo v6.2. rf represents the respiration fraction of the different transformation fluxes,  $\tau$**   
 521 **is the residence time (reciprocal of the rate constants that is the turnover rate), IM/MI: immobilization/mineralization**  
 522 **fluxes, HR: heterotrophic respiration. Note that both the respiration fraction and the turnover rate parameters can be**  
 523 **adjusted through parameterization.**

524

525

526 For the calculation of nitrogen mineralization first respiration cost (respiration  
 527 fraction) is estimated. Mineralization than is the function of the remaining part of the pool and  
 528 its C:N ratio. The nitrogen mineralization fluxes of the SOM pools are functions of the  
 529 potential rate constant (reciprocal of residence time), and the integrated response function that  
 530 accounts for the impact of multiple environmental factors. The integrated response function of  
 531 decomposition is a product of the response functions of depth, soil temperature and SWC  
 532 ( $F_r(d)_D$ ,  $F_r(T)_D$ ,  $F_r(SWC)_D$ ; Figure 5). Its detailed description can be found in the  
 533 Supplementary material, Section 7. The dependence of the three different factors on depth,  
 534 temperature and SWC with default parameters are presented in Figure 5.



535

536 **Figure 5:** The dependence of the individual factors that form the complex environmental response function of  
537 decomposition on depth ( $Fr(d)_b$ ), temperature ( $Fr(T)_b$ ) and SWC in case of different soil types ( $Fr(SWC)_b$ ). ED is the  
538 e-folding depth which is one of the adjustable soil parameters of the model. Sand soil means 92% sand, 4% silt and  
539 4% clay; silt soil means 8% sand, 86% silt and 6% clay; clay soil means 20% sand, 20% silt and 60% clay.

540

#### 541 4.3 Soil nitrogen processes

542 In Biome-BGCMuSo v6.2 separate ammonium ( $sNH_4$ ) and nitrate ( $sNO_3$ ) soil pools  
543 are implemented instead of a general mineralized nitrogen pool. This was a necessary step for



544 the realistic representation of many internal processes like plant nitrogen uptake, nitrification,  
545 denitrification, consideration of the effect of different mineral and organic fertilizers and N<sub>2</sub>O  
546 emission.

547 It is important to introduce the *availability* concept that Biome-BGCMuSo uses and is  
548 associated with the ammonium and nitrate pools. We use the logic proposed by Thomas et al.  
549 (2013) which means that the plant has access only to a part of the given inorganic nitrogen  
550 pool. Unavailable part is buffered as it is associated with soil aggregates and is unavailable for  
551 plant uptake. The available part of ammonium is calculated based on *NH<sub>4</sub> mobilen proportion*  
552 (that is a soil parameter set to 10% according to Thomas et al., 2013; Hidy et al., 2021) and  
553 the actual pool. The available part of nitrate is assumed to be 100%.

554 The amount of ammonium and nitrate are determined layer by layer controlled by  
555 input and output fluxes ( $F$  in kg N m<sup>-2</sup> day<sup>-1</sup>) listed below:

$$556 F_{sNH_4}^i = IN_{sNH_4}^i - L_{sNH_4}^i + L_{sNH_4}^{i-1} - PU_{sNH_4}^i - IM_{sNH_4}^i + MI_{sNH_4}^i - NI_{sNH_4}^i \quad (8)$$

$$557 F_{sNO_3}^i = IN_{sNO_3}^i - L_{sNO_3}^i + L_{sNO_3}^{i-1} - PU_{sNO_3}^i - IM_{sNO_3}^i + MI_{sNO_3}^i - DN_{sNO_3}^i \quad (9)$$

558 where  $IN_{sNH_4}^i$  and  $IN_{sNO_3}^i$  are the input fluxes to the ammonium and nitrate pools, respectively;  
559  $L_{sNH_4}^i$ ,  $L_{sNH_4}^{i-1}$ ,  $L_{sNO_3}^i$ ,  $L_{sNO_3}^{i-1}$  are the amount of leached mineralized ammonium and nitrate from  
560 a layer ( $i$ ) or from the upper layer ( $i-1$ ), respectively;  $PU_{sNH_4}^i$  and  $PU_{sNO_3}^i$  are the plant uptake  
561 fluxes of ammonium and nitrate, respectively;  $IM_{sNH_4}^i$  and  $IM_{sNO_3}^i$  are the immobilization  
562 fluxes of ammonium and nitrate, respectively;  $MI_{sNH_4}^i$  and  $MI_{sNO_3}^i$  are the mineralization  
563 fluxes of ammonium and nitrate, respectively;  $NI_{sNH_4}^i$  is the nitrification flux of ammonium  
564 and  $DN_{sNO_3}^i$  is the denitrification flux of nitrate.

565 In the following subsections the different terms of the equations are described in  
566 detail.

#### 567 Input to the sNH<sub>4</sub> and sNO<sub>3</sub> pools (IN in Eq. 6 and 7)

568 According to the model logic N-fixation occurs in the root zone layers. Its distribution  
569 between sNH<sub>4</sub> and sNO<sub>3</sub> pools is calculated based on their actual available proportion in the  
570 actual layer ( $NH_4prop^i$ ):

$$571 NH_4prop^i = sNH_4avail^i + sNO_3avail^i \quad (10)$$

572 where  $sNH_4avail^i$  and  $sNO_3avail^i$  are the available part of the sNH<sub>4</sub> and sNO<sub>3</sub> pools in the  
573 actual layer.

574 N-deposition related nitrogen input is associated with the 0-10 cm soil layers assuming  
575 uniform distribution across layers 1-2 in the model, and the distribution between sNH<sub>4</sub> and



576 sNO<sub>3</sub> pools is calculated based on the *proportion of NH<sub>4</sub> flux of N-deposition* soil parameter  
577 (Hidy et al., 2021).

578 Organic and inorganic fertilization is also an optional nitrogen input. The amount and  
579 composition (NH<sub>4</sub><sup>+</sup> and NO<sub>3</sub><sup>-</sup> content) can be set in the fertilization input file.

580

#### 581 Leaching - downward movement of mineralized N (L in Eq. 6 and 7)

582 The amount of leached mineralized N (mobile part of the given N pool) from a layer is  
583 directly proportional to the amount of drainage and the available part of the sNH<sub>4</sub> and sNO<sub>3</sub>  
584 pools. Leaching from the layer above is a net gain, while leaching from actual layer is a net  
585 loss for the actual layer. Leaching is described in Section 4.5.

586

#### 587 Plant uptake by roots (PU in Eq. 6 and 7)

588 N uptake required for plant growth is estimated in the photosynthesis calculations and  
589 the amount is distributed across the layers in the root zone. The partition of the N uptake  
590 between sNH<sub>4</sub> and sNO<sub>3</sub> pools is calculated based on their actual available proportion in each  
591 layer.

592

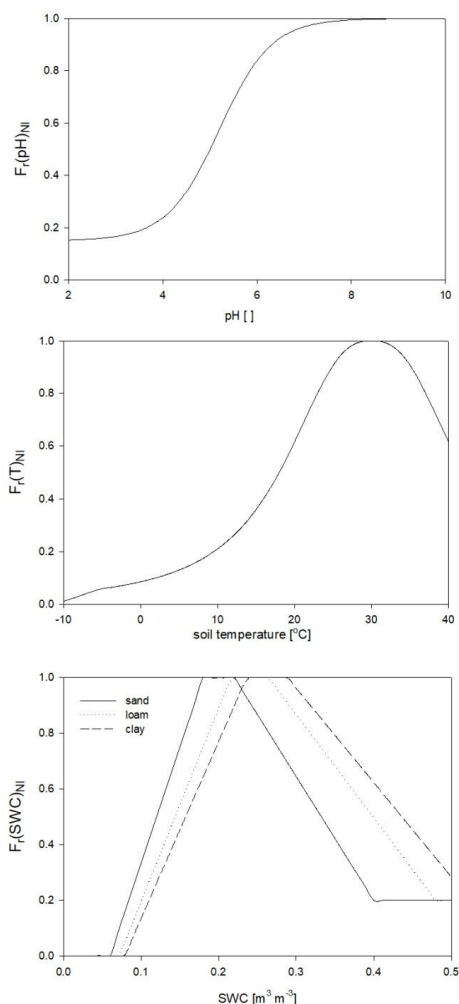
#### 593 Mineralization and immobilization (MI and IM Eq. 6 and 7)

594 Mineralization and immobilization calculations are detailed in Section 4.2. The  
595 distribution of these N fluxes between sNH<sub>4</sub> and sNO<sub>3</sub> pools is calculated based on their  
596 actual available proportion in each layer.

597

#### 598 Nitrification (NI Eq. 6 and 7)

599 Nitrification is a function of the soil ammonium content, the net mineralization and the  
600 response functions of temperature, soil pH and SWC ( $F_r(pH)_{NI}$ ,  $F_r(T)_{NI}$ , and  $F_r(SWC)_{NI}$ ,  
601 respectively) based on the method of Parton et al. (2001) and Thomas et al. (2013). Its  
602 detailed mathematical description can be found in the Supplementary material, Section 8. The  
603 response functions with proposed parameters are shown in Figure 6.



604

605 **Figure 6: The dependence of the individual factors of the environmental response function of nitrification on soil pH**  
 606 **( $F_r(\text{pH})_{\text{NI}}$ ), temperature ( $F_r(T)_{\text{NI}}$ ) and SWC  $F_r(\text{SWC})_{\text{NI}}$  in case of different soil types. pH and temperature response**  
 607 **functions are independent of the soil texture.**

608

609 Denitrification (DN Eq. 6 and 7)

610 Denitrification flux is estimated with a simple formula (Thomas et al., 2013):

$$611 \quad DN^i = DNcoeff \cdot SOMresp^i \cdot sNO3avail^i \cdot WFPS^i \quad (11)$$

612 where  $DN$  of the actual layer is the product of the available nitrate content ( $sNO3avail$  in  
 613  $\text{kg N m}^{-2}$ ),  $SOMresp^i$  in  $\text{g C m}^{-2} \text{day}^{-1}$  is the SOM decomposition related respiration cost, the  
 614  $WFPS^i$  is the water-filled pore space and  $DNcoeff$  is the *soil respiration related*  
 615 *denitrification rate* in  $\text{g C}^{-1}$ , which is an input soil parameter (Hidy et al., 2021). The unitless



616 water-filled pore space is the ratio of the actual and the saturated SWC. SOM decomposition  
617 associated respiration is the sum of the heterotrophic respiration fluxes of the four soil  
618 compartments (S1-S4, Figure 4.).

619

#### 620 **4.4 N<sub>2</sub>O-emission and N-emission**

621

622 During both nitrification and denitrification N<sub>2</sub>O-emission occurs which (added to the  
623 N<sub>2</sub>O-flux originated from grazing processes if applicable) contributes to the total N<sub>2</sub>O-  
624 emission of the examined ecosystem.

625 In Biome-BGCMuSo v6.2 a fixed part (set by the *coefficient of N<sub>2</sub>O emission of*  
626 *nitrification* input soil parameter; Hidy et al., 2021) of nitrification flux is lost as N<sub>2</sub>O and not  
627 converted to NO<sub>3</sub>.

628 During denitrification, nitrate is transformed into N<sub>2</sub> and N<sub>2</sub>O gas depending on the  
629 environmental conditions: NO<sub>3</sub> availability, total soil respiration (proxy for microbial  
630 activity), SWC and pH. The *denitrification related N<sub>2</sub>/N<sub>2</sub>O ratio* input soil parameter is used  
631 to represent the effect of the soil type on the N<sub>2</sub>/N<sub>2</sub>O ratio (del Grosso et al., 2000; Hidy et al.,  
632 2021). Detailed mathematical description of the algorithm can be found in the Supplementary  
633 material, Section 9.

634

#### 635 **4.5 Leaching of dissolved matter**

636 Leaching of nitrate, ammonium, and dissolved organic carbon and nitrogen (DOC and  
637 DON) content from the actual layer is calculated as the product of the concentration of the  
638 dissolved component in the soil water and the amount of water (drainage plus diffusion)  
639 leaving the given layer either downward or upward. The dissolved component (concentration)  
640 of organic carbon is calculated from the SOC pool contents and the corresponding *fraction of*  
641 *dissolved part of SOC* soil parameters. The dissolved component of organic nitrogen content  
642 of the given soil pool is calculated from the carbon content and the corresponding C:N ratio.  
643 The downward leaching is net loss from the actual layer and net gain for the layer next below;  
644 the upward flux is net loss for the actual layer and net gain for the layer next up. The  
645 downward leaching of the bottom active layer (9<sup>th</sup>) is net loss for the system. The upward  
646 movement of dissolved substance from the passive (10<sup>th</sup>) layer is net gain for the system.





647 **5. Case studies**

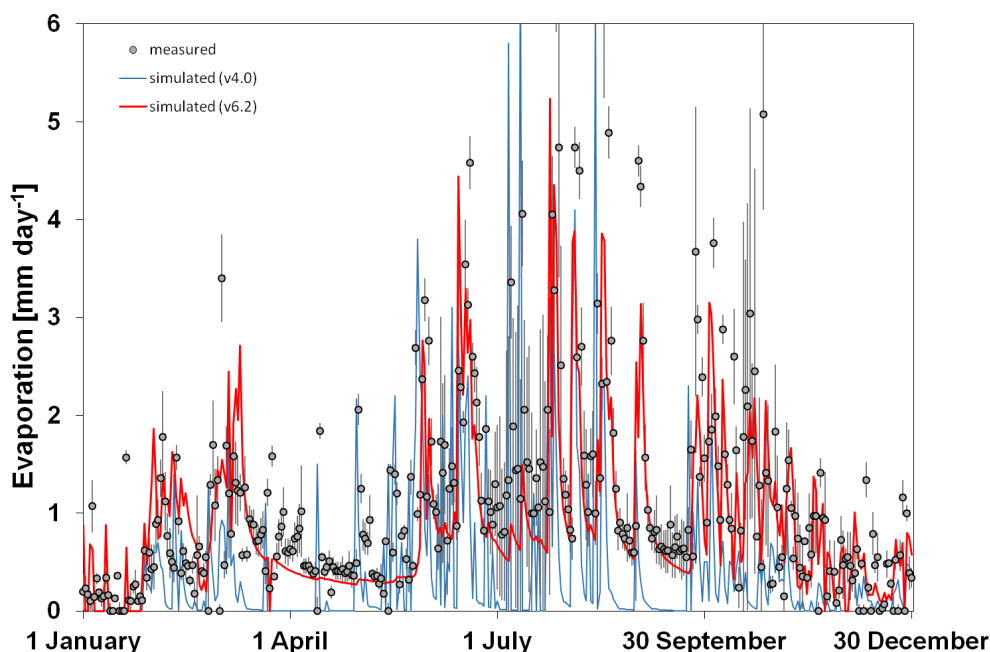
648 **5.1 Evaluation of soil hydrological simulation**

649 In order to evaluate the functioning of the new model version (and to compare  
650 simulation results made by the current and the previously published model version), a case  
651 study is presented regarding soil water content and soil evaporation simulations. The results  
652 of a bare soil simulation (i.e. no plant is assumed to be present) are compared to observation  
653 data of a weighing lysimeter station installed at Martonvásár, Hungary (47°18'57.6"N,  
654 18°47'25.6"E) in 2017. The station consists of twelve 2 meter deep scientific lysimeter  
655 columns with 1 m diameter (Meter Group Inc., USA) with soil temperature, SWC and soil  
656 water potential sensors installed at 5, 10, 30, 50, 70, 100 and 150 cm depth. Observation data  
657 for 2020 from six columns without vegetation cover (i.e. bare soil) was used to validate the  
658 model.

659 Raw lysimeter observation data were processed using standard methods. Bare soil  
660 evaporation values were derived based on changes of the mass of the soil columns also  
661 considering the mass change of the drainage water. Additionally, experience has shown that  
662 wind speed is related to the high frequency mass change of the soil column mass. To reduce  
663 noise, 5-point (5-min) moving averages were used based on Marek et al. (2014). After quality  
664 control of the data, the corrected and smoothed lysimeter mass values were used for the  
665 calculations. SWC observations were averaged to daily resolution to match the time step of  
666 the model.

667 Observed local meteorology was used to drive the models for year 2020. Soil physical  
668 model input parameters (field capacity, wilting point, bulk density, etc.) were determined in  
669 the laboratory using 100 cm<sup>3</sup> undisturbed soil samples taken from various depths during the  
670 installation of the lysimeter station. Regarding other soil parameters the proposed values were  
671 used. Detailed description of the input soil parameters and their proposed values are presented  
672 in the User's Guide (Hidy et al., 2021).

673 In Figure 7 the simulated and the observed time series of soil evaporation are  
674 presented for Martonvásár, for 2020. The figure shows that the soil evaporation simulation by  
675 v6.2 is more realistic than by v4.0. Biome-BGCMuSo v4.0 provides very low values during  
676 summer in some days which is not in accordance with the observations. Biome-BGCMuSo  
677 v6.2 provides more realistic values during this time period.



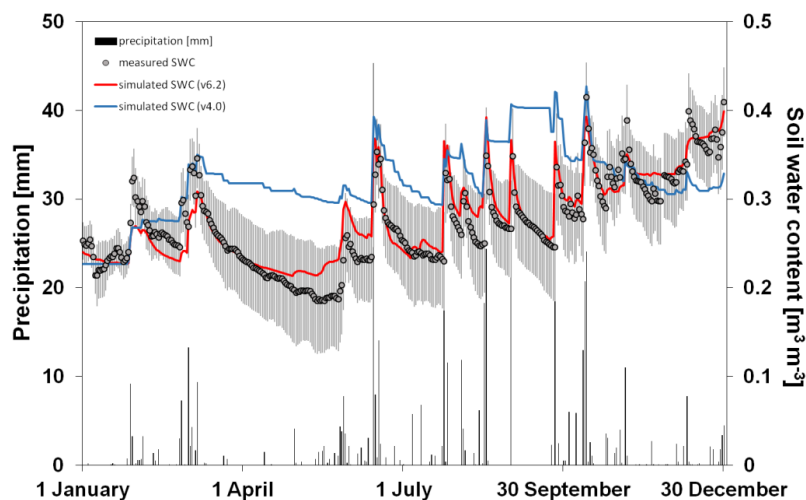
678

679 **Figure 7: The simulated (blue line: v4.0; red line: v6.2) and the observed (grey dots) daily soil evaporation values at**  
680 **Martonvásár during 2020. Vertical grey lines associated with the observations represent standard deviation of the**  
681 **observation from 6 columns. The improved model clearly outperforms the earlier version.**

682

683

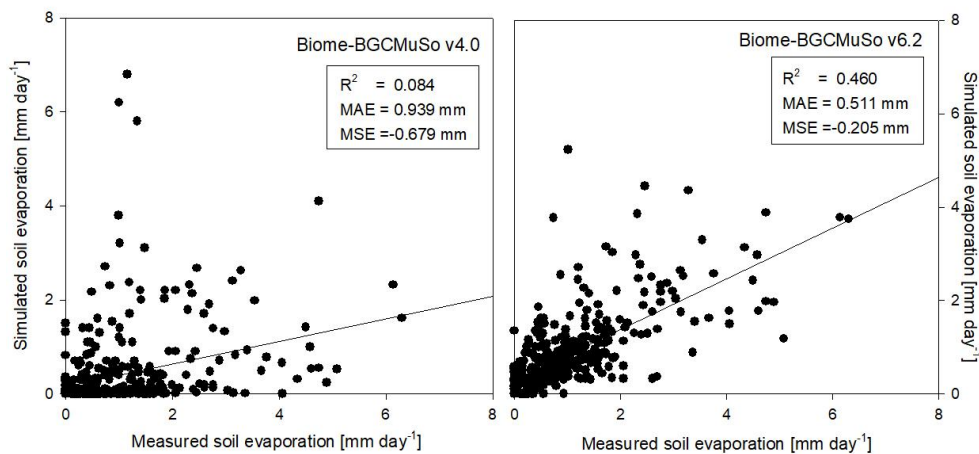
684 In Figure 8 the simulated and the observed SWC at 10 cm depth are presented with the  
685 daily sum of precipitation representing the bare soil simulation in Martonvásár, for 2020. The  
686 soil water balance simulation seems to be realistic using v6.2, since the annual course  
687 captures the low and high end of the observed values. In contrast, Biome-BGCMuSo v4.0  
688 underestimates the range of SWC and provides overestimations during the growing season  
689 (from spring to autumn). With a couple of exceptions, the simulated values using v6.2 fall  
690 into the uncertainty range of the measured values defined by the standard deviation of the six  
691 parallel measurements. This is not the case for the simulations with the 4.0 version.



692

693 **Figure 8:** The simulated (blue line: v4.0; red line: v6.2) and the observed (gray dots) soil water content values at 10 cm  
 694 depth (right y axis) with the daily sums of precipitation (left axis; black columns) during 2020 at Martonvásár  
 695 lysimeter station. Vertical grey lines associated with the observations represent +/- one standard deviation of the  
 696 observation. Simulated SWC using v6.2 is more consistent with the observations than using v4.0.

697



698

699 **Figure 9:** Comparison of the simulated (left: v4.0; right: v6.2) and observed daily soil evaporation (right) representing  
 700 the means of measured data obtained from six weighing lysimeter columns with bare soil at Martonvásár in 2020.  $R^2$ ,  
 701 MAE and MSE denote the square of the linear correlation coefficient, mean absolute error and mean signed error  
 702 (bias) of the simulated values, respectively.

703

704

705

Model performance was evaluated by quantitative measures such as square of linear  
 706 correlation coefficient ( $R^2$ ), mean absolute error (MAE) and mean signed error (MSE). In  
 707 Figure 9 the comparison of the simulated and the observed daily evaporation is presented.

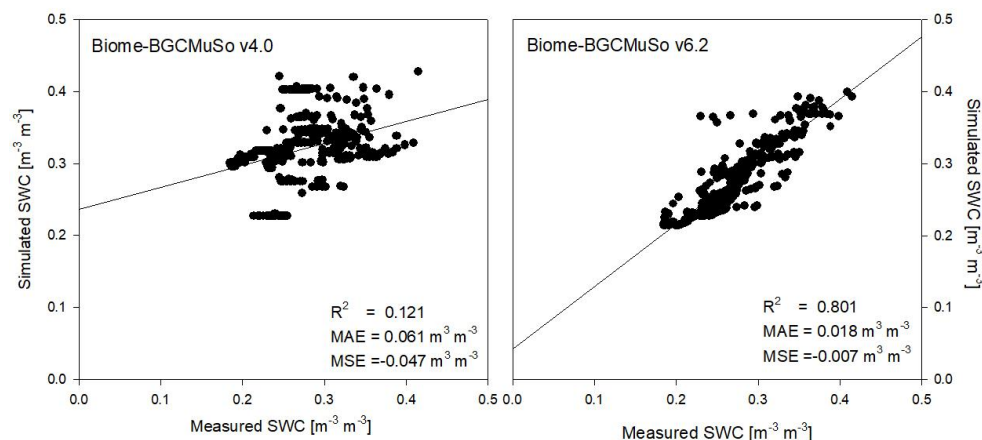


708 Based on the performance indicators it is obvious that the simulation with new model version  
709 (v6.2) is much closer to observations than the old version (v4.0). Biome-BGCMuSo v6.2  
710 slightly underestimated the observations.

711 In Figure 10 the comparison of the simulated and the observed daily SWC from the  
712 lysimeter experiment is presented. Based on the model evaluation it seems that the simulation  
713 with new model version is much closer to observation than with old version (4.0). The results  
714 obtained from v4.2 are consistent with earlier findings about the incorrect representation of  
715 the annual SWC cycle (Hidy et al., 2016; Sándor et al., 2017).

716 Throughout validation of the improved model based on observed SWC and ET  
717 datasets from eddy covariance sites is under way.

718



719

720 **Figure 10:** Comparison of the simulated (left: v4.0; right: v6.2) and observed daily SWC representing the means of  
721 measured data obtained from six weighing lysimeter columns with bare soil at Martonvásár in 2020.  $R^2$ , MAE and  
722 MSE denote the square of the linear correlation coefficient, mean absolute error and mean signed error (bias) of the  
723 simulated values, respectively.

724

725

## 726 5.2 Sensitivity analysis and optimization of the soil biogeochemistry scheme

727

728 Here we present another case study that provides insight into the functioning of the  
729 converging cascade scheme that is implemented in Biome-BGCMuSo v6.2. A large scale  
730 experiment is also presented where the main aim was to perform model self-initialization (i.e.  
731 spinup) at the country scale (for the entire area of Hungary) where the resulting soil organic  
732 matter pools are expected to be consistent with the observations.



733           The observation based, gridded, multi-layer SOC database of Hungary (DOSoReMI  
734 database; Pásztor et al., 2020) as well as the FORESEE meteorological database (Kern et al.,  
735 2016) was used for the sensitivity analysis of the soil scheme as well as for optimizing the  
736 most important soil parameters referring to SOC simulation. As a first step, the area of the  
737 country was divided into 1104 grid cells (regular grid with 0.1° by 0.1° resolution). The 1104  
738 grid cells of the DOSoReMI database were grouped based on their dominant land-use type  
739 (cropland, grassland, forest based on CORINE-2012 database; EEA, 2021) as well as the soil  
740 texture class (12 classes according to the USDA system; USDA, 1987) and SOC content (high  
741 and low; high is greater than the group mean while low is less than the mean) of the topsoil  
742 (0-30 cm layer). As some of the theoretically possible 72 groups had no members (e.g. there is  
743 no soil in Hungary with sandy-clay texture) soils of the 1104 grid cells were categorized into  
744 51 groups. For each group one single cell (so-called representative cell) was selected based on  
745 the topsoil SOC content. The representative cell was the one with the smallest absolute  
746 deviation from the group mean SOC content.

747           Grassland ecophysiological parameterization without management was used for  
748 croplands for the spinup phase, and with fertilization, harvest and ploughing settings in the  
749 transient phase. In case of grasslands, both during the spinup and transient phases grassland  
750 parameterization was used, and in the transient phase mowing was assumed (once a year in  
751 case of forests generic deciduous broadleaf forest parameterization was used for both spinup  
752 and transient phases, and in the transient phase thinning was set. Parameterization was  
753 performed based on generic, plant functional type specific ecophysiological parameters that  
754 were created based on the original parameterization of White et al. (2000). Biome-BGCMuSo  
755 specific parameter sets are available at the website of the model<sup>1</sup>.

756           Soil parameters in Biome-BGCMuSo 6.2 were classified into six groups: (1) 4 generic  
757 soil parameters, (2) 24 decomposition-nitrification-denitrification related parameters, (3) 14  
758 rate scalars for the converging cascade scheme, (4) 19 soil moisture related parameters, (5) 7  
759 methane related parameters and (6) 11 soil composition and characteristic values (can be set  
760 layer by layer). Detailed description and proposed value of each soil parameters can be found  
761 in the User's Guide (Hidy et al., 2021).

762  
763

---

<sup>1</sup> [http://nimbus.elte.hu/bbgc/files/generic\\_EPC\\_set\\_6.1.zip](http://nimbus.elte.hu/bbgc/files/generic_EPC_set_6.1.zip)



764 **Table 1: Soil parameters of Biome-BGCMuSo v6.2 (referring to SOC simulation) that were used during the sensitivity**  
 765 **analysis. The first column contains the group, the second contains the name of the parameter, the third contains the**  
 766 **abbreviation, and the fourth contains original proposed values (Hidy et al., 2021). See Figure 4 for explanation on the**  
 767 **compartment names. The parameters that were included in the 2<sup>nd</sup> phase of the sensitivity analysis are marked with**  
 768 **bold letters (see text).**

GROUP	NAME	ABBREVIATION	VALUE
Generic soil parameters	<b>C:N ratio of stable soil pool (soil4)</b>	<b>soil4CN</b>	<b>12</b>
	NH4 mobilien proportion	amMP	0.1
	aerodynamic resistance	potRair	107
Decomposition, nitrification, denitrification parameters	<b>parameter 1 for temperature response function of decomp.</b>	<b>Tp1decomp</b>	<b>1.75</b>
	<b>parameter 2 for temperature response function of decomp.</b>	<b>Tp2decomp</b>	<b>17</b>
	<b>parameter 3 for temperature response function of decomp.</b>	<b>Tp3decomp</b>	<b>2.6</b>
	<b>parameter 4 for temperature response function of decomp.</b>	<b>Tp4decomp</b>	<b>40</b>
	<b>minimum T for decomposition and nitrification</b>	<b>Tp5decomp</b>	<b>-5</b>
	e-folding depth of decomposition rate's depth scalar	EFD	10
	net mineralization proportion of nitrification	NITRnetMINER	0.2
	maximum nitrification rate	NITRmaxRATE	0.1
	coefficient of N2O emission of nitrification	NITRratioN2O	0.02
	parameter 1 for pH response function of nitrification	pHp1nitrif	0.15
	parameter 2 for pH response function of nitrification	pHp2nitrif	1
	parameter 3 for pH response function of nitrification	pHp3nitrif	5.2
	parameter 4 for pH response function of nitrification	pHp4nitrif	0.55
	parameter 1 for Tsoil response function of nitrification	Tp1nitrif	1
	parameter 2 for Tsoil response function of nitrification	Tp2nitrif	12
	parameter 3 for Tsoil response function of nitrification	Tp3nitrif	2.6
	parameter 4 for Tsoil response function of nitrification	Tp4nitrif	2.6
	minimum WFPS for scalar of nitrification calculation	minWFPS	0.1
	lower optimum WFPS for scalar of nitrification	opt1WFPS	0.45
	higher optimum WFPS for scalar of nitrification	opt2WFPS	0.55
	minimum value for saturated WFPS scalar of nitrification	minWFPSscalar	0.2
	<b>soil respiration related denitrification rate</b>	<b>DENITcoeff</b>	<b>0.05</b>
	denitrification related N2/N2O ratio multiplier	DNratioN2O	2
<b>critical WFPS value for denitrification</b>	<b>critWFPSdenitr</b>	<b>0.50</b>	
Rate scalars	<b>respiration fractions for fluxes between compartments (1s1)</b>	<b>RF1s1</b>	<b>0.39</b>
	<b>respiration fractions for fluxes between compartments (1s2)</b>	<b>RF1s2</b>	<b>0.55</b>
	<b>respiration fractions for fluxes between compartments (1s3)</b>	<b>RF1s3</b>	<b>0.29</b>
	<b>respiration fractions for fluxes between compartments (s1s2)</b>	<b>RFs1s2</b>	<b>0.28</b>
	<b>respiration fractions for fluxes between compartments (s2s3)</b>	<b>RFs2s3</b>	<b>0.46</b>
	<b>respiration fractions for fluxes between compartments (s3s4)</b>	<b>RFs3s4</b>	<b>0.55</b>
	potential rate constant of labile litter pool	RCS1	0.7
	potential rate constant of cellulose litter pool	RCS2	0.07
	potential rate constant of lignin litter pool	RCS3	0.014
	potential rate constant of fast microbial recycling pool	RCS4	0.07
	potential rate constant of medium microbial recycling pool	RCS5	0.014
	<b>potential rate constant of slow microbial recycling pool</b>	<b>RCS6</b>	<b>0.0014</b>
	<b>potential rate constant of recalcitrant SOM (humus) pool</b>	<b>RCS7</b>	<b>0.0001</b>
	potential rate constant of physical fragmentation of wood	RCS8	0.001
	maximum height of pond water	MP	5
	<b>curvature of soil stress function</b>	<b>q</b>	<b>1</b>
	fraction of dissolved part of S1 organic matter	fD1	0.005
	fraction of dissolved part of S2 organic matter	fD2	0.004
	<b>fraction of dissolved part of S3 organic matter</b>	<b>fD3</b>	<b>0.003</b>
	<b>fraction of dissolved part of S4 organic matter</b>	<b>fD4</b>	<b>0.002</b>
	mulch parameter: critical amount	CAmulch	1
	parameter 1 for mulch function	p1mulch	100
	parameter 2 for mulch function	p2mulch	0.75
	parameter 3 for mulch function	p3mulch	0.75
	mulch parameter: evaporation reduction	ERmulch	0.5



769 As methane simulation was not the subject of the present case study we neglected the  
770 related parameters. Regarding to the soil composition and characteristic values we used the  
771 DOSoReMI database (Pásztor et al., 2020). From the remaining 61 parameters soil depth,  
772 runoff curve number, the three soil moisture related parameters (tipping bucket method) were  
773 not included into analysis. Groundwater parameters were inactive in this case (no  
774 groundwater is assumed) which means that those parameters were not studied. The remaining  
775 53 parameters are used in sensitivity analysis and are listed in Table 1.

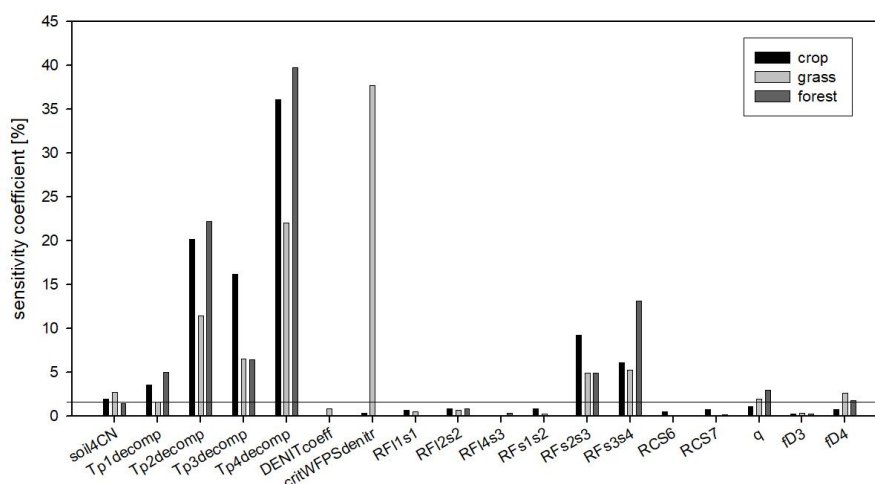
776 As a first step sensitivity analysis was carried out for the selected 53 soil parameters  
777 by running the Biome-BGCMuSo v6.2 model in spinup mode until a quasi-equilibrium in the  
778 total SOC is reached (that is the usual logic of the spinup run). The model was run for each  
779 representative cell 2000 times with varying model parameters using Monte-Carlo method.  
780 Each model parameters were varied randomly within the  $\pm 10\%$  range of their initial values  
781 that were inherited from the Biome-BGC model or were set according to the literature. The  
782 least square linearization (LSL) method (Verbeeck et al., 2006) was used for dividing output  
783 uncertainty into its input parameter related variability. As result of the LSL method, the total  
784 variance of the model output and the sensitivity coefficient of each parameter can be  
785 determined. Sensitivity coefficients show the percent of total variance for which the given  
786 parameter is responsible.

787 In order to simplify the workflow and decrease the degree of freedom another  
788 sensitivity analysis was performed. In this second step, the sensitive parameters (sensitivity  
789 coefficient  $> 1\%$  for at least one land use type; a total of 18 parameters) were used in the  
790 following sensitivity analysis with 6000 iteration steps. These 18 parameters are marked with  
791 bold letters in Table 1.

792 Figure 10 shows the summary of the second sensitivity analysis where the overall  
793 importance of the parameters are calculated as the mean of all selected pixels in a given land  
794 use category. It can be seen in Figure 10 that from the 18 parameters (selected during the first  
795 phase) soil carbon ratio of the recalcitrant pool (soil4CN), the temperature dependence  
796 parameters of decomposition function (Tp1decomp, Tp2decomp, Tp3decomp, Tp4\_decomp)  
797 and the respiration fraction of S2-S3 and S3-S4 decomposition process (RFs2s3 and RFs3s4),  
798 the curvature of soil stress function ( $q_{\text{soilstress}}$ ) and the fraction of dissolved part of S4 organic  
799 matter (fD4) are the most important for all land use types. Among the other parameters the  
800 critical WFPS of denitrification (critWFPSdentir) for grasslands has a remarkably high  
801 sensitivity (greater than 35%). It means that in case of grasslands the nitrogen availability  
802 seems to be an important limitation of the primary production, probably because there are



803 only natural sources of nitrogen (no fertilization is assumed here), and the rooting zone is  
 804 shallower than in case of forest which involves limited mineralized N access. Thus, in case of  
 805 higher values of critical WFPS of denitrification, the simulated production of the grassland  
 806 (and therefore the final SOC) seems to be significantly underestimated.



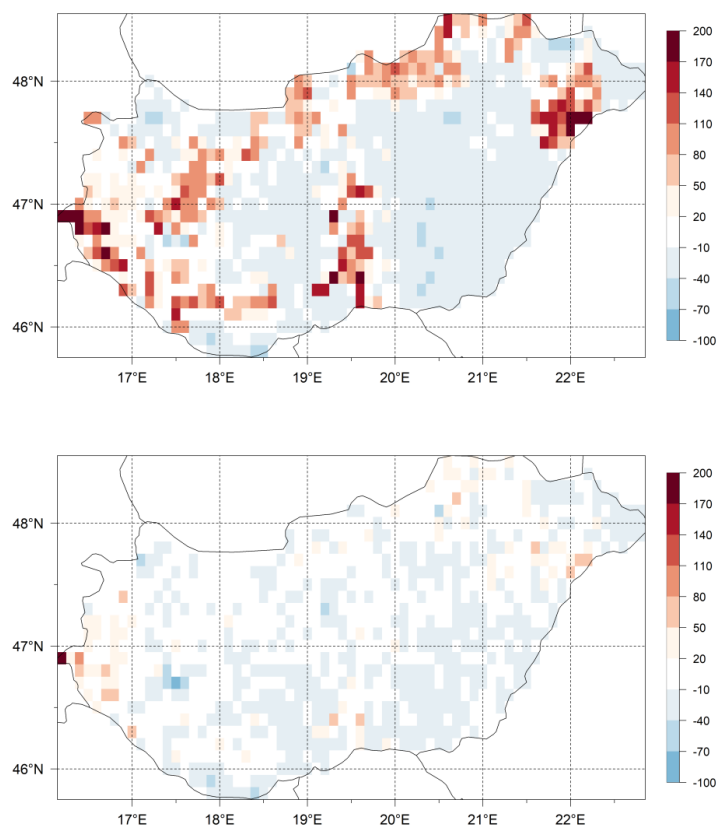
807  
 808 **Figure 10: The sensitivity coefficients of the soil parameters as the result of the sensitivity analysis. Black columns**  
 809 **refer to the crop, light grey to the grass and dark grey to the forest simulations. The sensitivity coefficients are**  
 810 **calculated as the mean pixel level sensitivity coefficient for the given land use type. Horizontal line indicates the 5%**  
 811 **threshold that was used to select the final parameter set that is subject to optimization.**

812

813 The selected ten, soil biogeochemistry related parameters were optimized for each of  
 814 the 51 groups separately, using maximum likelihood estimation. For each group, the  
 815 parameter set providing the smallest deviation between the simulated and the observed values  
 816 of the weighted average SOC content (weight factor of 5 is used for the 0-30 cm, and weight  
 817 factor of 1 is used for the 30-60 cm soil layers) was considered to be the final (optimized)  
 818 model parameter set.

819 The differences of the simulated and observed SOC content for the 0-30 cm layer  
 820 (SOC0-30) using the initial (Table 1) and final soil parameters (not shown here) are presented  
 821 in Figure 11. On the upper plot the signed relative error of SOC0-30 simulation before  
 822 optimization, while on the lower figure the signed relative error of SOC0-30 simulation after  
 823 optimization can be seen. It is clearly visible that because of optimization the overestimation  
 824 of the SOC0-30 simulation significantly decreased.





825

826 **Figure 11: Differences between the simulated and observed SOC data for the 0-30 layer (SOC0-30) using the initial**  
827 **(upper map) and optimized (lower map) soil parameters. The maps present the signed relative error in percent.**  
828 **Visual comparison of the maps reveals the success of the optimization in terms of capturing the overall SOC for the**  
829 **country area.**

830

831 We do not claim of course that the optimized parameters have universal value. Site  
832 history is neglected during the spin up simulations, and we use many simplifications like non-  
833 existent land use change, present-day ecophysiological parameterization etc. In this sense,  
834 the optimized parameter set can be best considered as a pragmatic solution to provide initial  
835 conditions (equilibrium SOC pools) for the model at the country scale that is consistent with  
836 the observations.



837 **6. Concluding remarks**

838 In this paper, we presented a detailed description of the soil hydrology and  
 839 carbon/nitrogen budget related developments of the Biome-BGCMuSo v6.2 terrestrial  
 840 ecosystem model. We mostly focused on changes relative to the previously published Biome-  
 841 BGCMuSo v4.0 (Hidy et al., 2016), but our intention was also to provide a complete,  
 842 standalone reference for the modelling community with mathematical equations (detailed in  
 843 the Supplementary Material). Table 2 summarizes the structural changes that we made during  
 844 the developments starting from Biome-BGC v4.1.1 also including the previously published  
 845 Biome-BGCMuSo v4.0 (Hidy et al., 2016).

846

847 **Table 2. Comparison of model structural solutions for Biome-BGC 4.1.1, Biome-BGCMuSo v4.0 and Biome-**  
 848 **BGCMuSo v6.2.**

Routine	original Biome-BGC	Biome-BGCMuSo v4.0	Biome-BGCMuSo v6.2
Runoff	no	based on simple, empirical formulation	distinguishing Hortonian and Dunne runoff
Pond water	no	simple solution	development of pond water formation (based on infiltration capacity)
Soil evaporation	Based on Penman-Monteith equation Calculation of the actual evaporation from the potential evaporation and the square root of time elapsed since the last precipitation.	Based on Penman-Monteith equation Calculation of the actual evaporation from the potential evaporation and the square root of time elapsed since the last precipitation.	Based on Penman-Monteith equation Parameterization possibility of actual aerodynamic resistance. Introduction of an upper limit for daily potential evaporation that is determined by the available energy. Calculation of the actual evaporation is based on the method Ritchie (1981). Simulation of the reducing effect of surface residue or mulch cover on bare soil evaporation
Transpiration	Transpiration from one-layer bucket soil	Transpiration from 7-layers soil based on soil stress	Transpiration from 10-layers soil based on available water
Groundwater	no	Simple groundwater simulation.	Improvement of the simulation of groundwater effect (using capillary fringe). Introduction of two different methods.
Soil moisture stress	no	Relative SWC data is used to calculate soil water stress. The hygroscopic water, the wilting point, the field capacity and the saturation values of the soil layers can be defined in the input file layer by layer. The soil moisture stress index is affected by the length and the day since the drought event lasted.	The hygroscopic water, the wilting point, the field capacity and the saturation values of the soil layers can be defined in the input file layer by layer. The soil moisture stress index is affected by the length and the severity of the drought event, aggravated by the extreme temperature. Introduction of the soil curvature parameters to provide mechanism for soil texture dependent drought stress since it can affect the shape of the soil stress function.



			Normalized SWC data are used to calculate soil moisture stress index.
Organic carbon and nitrogen	One layer soil module with one organic carbon and nitrogen pool.	Multi-layered soil module without soil carbon and nitrogen profile.	Instead of defining a single litter, soil organic carbon and nitrogen pool, separate carbon and nitrogen pools for each soil layer in the form of soil organic matter and litter were implemented. Separation of above- and belowground litter pools. Litter and soil decomposition fluxes (carbon and nitrogen fluxes from litter to soil pools) are calculated layer by layer, depending on the actual temperature and SWC of the corresponding layers. Leaching of dissolved organic carbon and nitrogen.
Inorganic nitrogen	One layer soil module with one mineralized N pool.	Multi-layer soil module with an empirical inorganic N-profile (no layer-by-layer calculations, only estimation of the subpools in the different soil layer based on the rootlength proportion).	Separation of ammonium (sNH <sub>4</sub> ) and nitrate (sNO <sub>3</sub> ) soil pools instead of a general mineralized nitrogen pool. Nitrification fluxes are calculated layer by layer, depending on the actual pH, temperature and SWC of the given layers. Denitrification fluxes are calculated layer by layer, depending on the depth, actual temperature and SWC of the given layers.

849

850

851

Earlier model versions used a soil hydrology scheme based on the Richards equation, but the results were not satisfactory. Sándor et al. (2017) presented results from the first major grassland model intercomparison project (executed within the frame of FACCE MACSUR) where Biome-BGCMuSo 2.2 was used. That study demonstrated the problems associated with proper representation of soil water content that was a common shortcoming of all included models. In the Hidy et al. (2016) paper, where the focus was on Biome-BGCMuSo v4.0, the SWC related figures clearly indicated problems with the simulations compared to observations. The SWC amplitude was not captured well which clearly influences drought stress, decomposition, and other SWC driven processes like nitrification and denitrification. For the latter two processes this is especially critical as they are associated with contrasting SWC regimes (nitrification is an aerobic, while denitrification is an anaerobic process). This is a good example for erroneous internal process representation that may lead to improper results. Note that the currently used functions for nitrification/denitrification are also subject to uncertainty that needs to be addressed in the future (Heinen, 2006). Nevertheless, the

862



865 presented model developments might contribute to a more realistic soil process simulations  
866 and improved results.

867 Algorithm ensemble approach is already implemented in Biome-BGCMuSo.  
868 Algorithm ensemble means that the user has more than one option for the representation of  
869 some processes. Biome-BGCMuSo v6.2 has alternative phenology routines (Hidy et al.,  
870 2012), two alternative methods for soil temperature (Hidy et al., 2016), soil hydrology  
871 (described in this study), photosynthesis and soil moisture stress calculation. We plan to  
872 extend the algorithm ensemble by providing alternative decomposition schemes to the model.  
873 One possibility is the implementation of a CENTURY-like structure (Koven et al., 2013) that  
874 is a promising direction and might improve the quality of the equilibrium (spin-up)  
875 simulations and the simulated N mineralization related to SOM decomposition. Reported  
876 problems related to the rapid decomposition of litter in the current model structure (Bonan et  
877 al., 2013) needs to be addressed in future model versions as well.

878 Plant growth and allocation related developments were not addressed in this study but  
879 of course has many inferences with the presented model logic (i.e. parameterization and  
880 related primary production defines the amount and quality of litter, etc.). A forthcoming  
881 publication will provide a comprehensive overview on the plant growth and senescence  
882 related model modifications where elements from crop models are also included.

883 Biome-BGCMuSo is still an open source model that can be freely downloaded from  
884 its website with a detailed User's Guide and other supplementary files. We also encourage  
885 users to test the so-called RBBGCMuso package (available at GitHub) that has many  
886 advanced features to support model application and optimization. A graphical environment,  
887 called AgroMo (also available at GitHub) was also developed around Biome-BGCMuSo to  
888 help users in carrying out simulations either with site specific plot scale data or with gridded  
889 databases representing large regions.

890

891

## 892 **Code and data availability**

893 The current version of Biome-BGCMuSo, together with sample input files and detailed User's  
894 Guide are available from the website of the model: <http://nimbus.elte.hu/bbgc/download.html>  
895 under the GPL-2 licence. Biome-BGCMuSo v6 is also available at GitHub:  
896 [https://github.com/bpbond/Biome-BGC/tree/Biome-BGCMuSo\\_v6](https://github.com/bpbond/Biome-BGC/tree/Biome-BGCMuSo_v6). The exact version of the  
897 model (v6.2 alpha) used to produce the results used in this paper is archived on Zenodo



898 (<https://doi.org/10.5281/zenodo.5761202>). Experimental data and model parameterization used  
899 in the study are available from the corresponding author upon request.

900

901

## 902 **Authors' Contributions**

903 Hidy developed Biome-BGCMuSo, maintained the source code and executed the sample  
904 simulations. The study was conceived and designed by Hidy, Barcza and Fodor, with  
905 assistance from Ács, Dobor and Hollós. It was directed by Hidy and Barcza. Ács and Dobor  
906 contributed with model benchmarking. Hollós participated with the construction of a  
907 modeling framework for Biome-BGCMuSo. Filep, Incze, Zacháry and Pásztor contributed  
908 with experimental data. Hidy, Barcza, Fodor and Merganičová prepared the manuscript and  
909 the supplement with contributions from all co-authors. All authors reviewed and approved the  
910 present article and the supplement.

911

912

## 913 **Acknowledgements**

914 The research was funded by the Széchenyi 2020 programme, the European Regional  
915 Development Fund and the Hungarian Government (GINOP-2.3.2-15-2016-00028). Also  
916 supported by grant "Advanced research supporting the forestry and wood-processing sector's  
917 adaptation to global change and the 4th industrial revolution", No.  
918 CZ.02.1.01/0.0/0.0/16\_019/0000803 financed by OP RDE". KM was also financed by the  
919 project: "Scientific support of climate change adaptation in agriculture and mitigation of soil  
920 degradation" (ITMS2014+ 313011W580) supported by the Integrated Infrastructure  
921 Operational Programme funded by the ERDF. We are grateful to Galina Churkina for  
922 reviewing this manuscript.

923

## 924 **References**

925 Asseng, S., Ewert, F., Rosenzweig, C., Jones, J.W., Hatfield, J.L., Ruane, A.C., Boote, K.J.,  
926 Thorburn, P.J., Rötter, R.P., Cammarano, D., Brisson, N., Basso, B., Martre, P.,  
927 Aggarwal, P.K., Angulo, C., Bertuzzi, P., Biernath, C., Challinor, A.J., Doltra, J.,  
928 Gayler, S., Goldberg, R., Grant, R., Heng, L., Hooker, J., Hunt, L.A., Ingwersen, J.,  
929 Izaurralde, R.C., Kersebaum, K.C., Müller, C., Naresh Kumar, S., Nendel, C.,  
930 O'Leary, G., Olesen, J.E., Osborne, T.M., Palosuo, T., Priesack, E., Ripoche, D.,  
931 Semenov, M.A., Shcherbak, I., Steduto, P., Stöckle, C., Stratonovitch, P., Streck, T.,



- 932 Supit, I., Tao, F., Travasso, M., Waha, K., Wallach, D., White, J.W., Williams, J.R.,  
933 Wolf, J., 2013. Uncertainty in simulating wheat yields under climate change. *Nature*  
934 *Climate Change* 3, 827–832. <https://doi.org/10.1038/nclimate1916>
- 935 Balsamo, G., Viterbo, P., Beljaars, A., van den Hurk, B., Hirschi, M., Betts, A.K., Scipal, K.,  
936 2009. A Revised Hydrology for the ECMWF Model: *Journal of Hydrometeorology*  
937 10, 623–643.
- 938 Bassu, S., Brisson, N., Durand, J.-L., Boote, K., Lizaso, J., Jones, J.W., Rosenzweig, C.,  
939 Ruane, A.C., Adam, M., Baron, C., Basso, B., Biernath, C., Boogaard, H., Conijn, S.,  
940 Corbeels, M., Deryng, D., De Sanctis, G., Gayler, S., Grassini, P., Hatfield, J., Hoek,  
941 S., Izaurralde, C., Jongschaap, R., Kemanian, A.R., Kersebaum, K.C., Kim, S.-H.,  
942 Kumar, N.S., Makowski, D., Müller, C., Nendel, C., Priesack, E., Pravia, M.V., Sau,  
943 F., Shcherbak, I., Tao, F., Teixeira, E., Timlin, D., Waha, K., 2014. How do various  
944 maize crop models vary in their responses to climate change factors? *Global Change*  
945 *Biology* 20, 2301–2320. <https://doi.org/10.1111/gcb.12520>
- 946 Berardi, D., Brzostek, E., Blanc-Betes, E., Davison, B., DeLucia, E.H., Hartman, M.D., Kent,  
947 J., Parton, W.J., Saha, D., Hudiburg, T.W., 2020. 21st-century biogeochemical  
948 modeling: Challenges for Century-based models and where do we go from here? *GCB*  
949 *Bioenergy* 12, 774–788. <https://doi.org/10.1111/gcbb.12730>
- 950 Dietze, M., 2013. Gaps in knowledge and data driving uncertainty in models of  
951 photosynthesis. *Photosynthesis research* 119. [https://doi.org/10.1007/s11120-013-](https://doi.org/10.1007/s11120-013-9836-z)  
952 [9836-z](https://doi.org/10.1007/s11120-013-9836-z)
- 953 Dolezal, F., Hernandez-Gomis, R., Matula, S., Gulamov, M., Miháliková, M., Khodjaev, S.,  
954 2018. Actual Evapotranspiration of Unirrigated Grass in a Smart Field Lysimeter.  
955 *Vadose Zone Journal* 17. <https://doi.org/10.2136/vzj2017.09.0173>
- 956 EEA, 2021. "Co ORdinated INformation on the Environment (CORINE) Land Cover 2012,  
957 Version 18.4. European Commission - Directorate-General for Internal Market,  
958 Industry, Entrepreneurship and SMEs (DG-GROW, data owner)." European  
959 Environment Agency (EEA, data custodian). URL: [http://land.copernicus.eu/pan-](http://land.copernicus.eu/pan-european/corine-land-cover/clc-2012)  
960 [european/corine-land-cover/clc-2012](http://land.copernicus.eu/pan-european/corine-land-cover/clc-2012). Accessed 17 February 2021.
- 961 Ewert, F., Rötter, R.P., Bindi, M., Webber, H., Trnka, M., Kersebaum, K.C., Olesen, J.E., van  
962 Ittersum, M.K., Janssen, S., Rivington, M., Semenov, M.A., Wallach, D., Porter, J.R.,  
963 Stewart, D., Verhagen, J., Gaiser, T., Palosuo, T., Tao, F., Nendel, C., Roggero, P.P.,  
964 Bartošová, L., Asseng, S., 2015. Crop modelling for integrated assessment of risk to  
965 food production from climate change. *Environmental Modelling & Software* 72, 287–  
966 303. <https://doi.org/10.1016/j.envsoft.2014.12.003>
- 967 Farquhar, G.D., von Caemmerer, S., Berry, J.A., 1980. A biochemical model of  
968 photosynthetic CO<sub>2</sub> assimilation in leaves of C<sub>3</sub> species. *Planta* 149, 78–90.  
969 <https://doi.org/10.1007/BF00386231>
- 970 Franke, J., Müller, C., Elliott, J., Ruane, A., Jägermeyr, J., Balkovič, J., Ciais, P., Dury, M.,  
971 Falloon, P., Folberth, C., François, L., Hank, T., Hoffmann, M., Izaurralde, R.,  
972 Jacquemin, I., Jones, C., Khabarov, N., Koch, M., Moyer, E., 2020. The GGCM  
973 Phase 2 experiment: Global gridded crop model simulations under uniform changes in  
974 CO<sub>2</sub>, temperature, water, and nitrogen levels (protocol version 1.0). *Geoscientific*  
975 *Model Development* 13, 2315–2336. <https://doi.org/10.5194/gmd-13-2315-2020>
- 976 Fodor, N., Pásztor, L., Szabó, B., Laborczi, A., Pokovai, K., Hidy, D., Hollós, R., Kristóf, E.,  
977 Kis, A., Dobor, L., Kern, A., Grünwald, T., Barcza, Z., 2021. Input database related  
978 uncertainty of Biome-BGCMuSo agro-environmental model outputs. *International*  
979 *Journal of Digital Earth*, 1–20. <https://doi.org/10.1080/17538947.2021.1953161>
- 980 Friedlingstein, P., Joel, G., Field, C.B., Fung, I.Y., 1999. Toward an allocation scheme for  
981 global terrestrial carbon models. *Global Change Biology* 5, 755–770.



- 982 <https://doi.org/10.1046/j.1365-2486.1999.00269.x>
- 983 Friedlingstein, P., Prentice, I., 2010. Carbon-climate feedbacks: A review of model and  
984 observation based estimates. *Current Opinion in Environmental Sustainability* 2, 251–  
985 257. <https://doi.org/10.1016/j.cosust.2010.06.002>
- 986 Heinen, M., 2006. Simplified denitrification models: Overview and properties. *Geoderma*  
987 133, 444–463. doi:10.1016/j.geoderma.2005.06.010
- 988 Hidy, D., Barcza, Z., Haszpra, L., Churkina, G., Pintér, K., Nagy, Z., 2012. Development of  
989 the Biome-BGC model for simulation of managed herbaceous ecosystems. *Ecological*  
990 *Modelling* 226, 99–119. <https://doi.org/10.1016/j.ecolmodel.2011.11.008>
- 991 Hidy, D., Barcza, Z., Marjanović, H., Ostrogović Sever, M.Z., Dobor, L., Gelybó, G., Fodor,  
992 N., Pintér, K., Churkina, G., Running, S., Thornton, P., Bellocchi, G., Haszpra, L.,  
993 Horváth, F., Suyker, A., Nagy, Z., 2016. Terrestrial ecosystem process model Biome-  
994 BGC MuSo v4.0: summary of improvements and new modeling possibilities.  
995 *Geoscientific Model Development* 9, 4405–4437. [https://doi.org/10.5194/gmd-9-4405-](https://doi.org/10.5194/gmd-9-4405-2016)  
996 2016
- 997 Hidy, D., Barcza, Z., Hollós, R., Thornton, P. and Running, S. W., Fodor, N.: User's Guide  
998 for Biome-BGC MuSo 6.2. Available online:  
999 [http://nimbus.elte.hu/bbgc/files/Manual\\_BBGC\\_MuSo\\_v6.2.pdf](http://nimbus.elte.hu/bbgc/files/Manual_BBGC_MuSo_v6.2.pdf)
- 1000 Hufkens, K., Basler, D., Milliman, T., Melaas, E.K., Richardson, A.D., 2018. An integrated  
1001 phenology modelling framework in r. *Methods in Ecology and Evolution* 9, 1276–  
1002 1285. <https://doi.org/10.1111/2041-210X.12970>
- 1003 Huntzinger, D.N., Schwalm, C., Michalak, A.M., Schaefer, K., King, A.W., Wei, Y.,  
1004 Jacobson, A., Liu, S., Cook, R.B., Post, W.M., Berthier, G., Hayes, D., Huang, M., Ito,  
1005 A., Lei, H., Lu, C., Mao, J., Peng, C.H., Peng, S., Poulter, B., Ricciuto, D., Shi, X.,  
1006 Tian, H., Wang, W., Zeng, N., Zhao, F., Zhu, Q., 2013. The North American Carbon  
1007 Program Multi-Scale Synthesis and Terrestrial Model Intercomparison Project – Part  
1008 1: Overview and experimental design. *Geoscientific Model Development* 6, 2121–  
1009 2133. <https://doi.org/10.5194/gmd-6-2121-2013>
- 1010 Jones, J.W., Antle, J.M., Basso, B., Boote, K.J., Conant, R.T., Foster, I., Godfray, H.C.J.,  
1011 Herrero, M., Howitt, R.E., Janssen, S., Keating, B.A., Munoz-Carpena, R., Porter,  
1012 C.H., Rosenzweig, C., Wheeler, T.R., 2017. Brief history of agricultural systems  
1013 modeling. *Agricultural Systems* 155, 240–254.  
1014 <https://doi.org/10.1016/j.agsy.2016.05.014>
- 1015 Keenan, T.F., Carbone, M.S., Reichstein, M., Richardson, A.D., 2011. The model–data fusion  
1016 pitfall: assuming certainty in an uncertain world. *Oecologia* 167, 587.  
1017 <https://doi.org/10.1007/s00442-011-2106-x>
- 1018 Kern, A., H. Marjanović, and Z. Barcza. 2016. Evaluation of the quality of NDVI3g dataset  
1019 against Collection 6 MODIS NDVI in Central-Europe between 2000 and 2013.  
1020 *Remote Sensing* 8 (11): 955. doi:10.3390/rs8110955
- 1021 Koven, C.D., Riley, W.J., Subin, Z.M., Tang, J.Y., Torn, M.S., Collins, W.D., Bonan, G.B.,  
1022 Lawrence, D.M., Swenson, S.C., 2013. The effect of vertically resolved soil  
1023 biogeochemistry and alternate soil C and N models on C dynamics of CLM4.  
1024 *Biogeosciences* 10, 7109–7131. <https://doi.org/10.5194/bg-10-7109-2013>
- 1025 Kuzyakov, Y., 2011. How to link soil C pools with CO<sub>2</sub> fluxes? *Biogeosciences* 8, 1523–  
1026 1537. <https://doi.org/10.5194/bg-8-1523-2011>
- 1027 Levis, S., 2010. Modeling vegetation and land use in models of the Earth System. *WIREs*  
1028 *Climate Change* 1, 840–856. <https://doi.org/10.1002/wcc.83>
- 1029 Marek, G. W., Evett, S. R., Gowda, P. H., Howell, T. A., Copeland, K. S., Baumhardt, R. L. ,  
1030 2014. Post-processing techniques for reducing errors in weighing lysimeter  
1031 evapotranspiration (ET) datasets. *American Society of Agricultural and Biological*





- 1032 Engineers 57, 499–515. <https://doi.org/10.13031/trans.57.10433>.
- 1033 Martínez-Vilalta, J., Sala, A., Asensio, D., Galiano, L., Hoch, G., Palacio, S., Piper, F.I.,  
1034 Lloret, F., 2016. Dynamics of non-structural carbohydrates in terrestrial plants: a  
1035 global synthesis. *Ecological Monographs* 86, 495–516.  
1036 <https://doi.org/10.1002/ecm.1231>
- 1037 Martre, P., Wallach, D., Asseng, S., Ewert, F., Jones, J.W., Rötter, R.P., Boote, K.J., Ruane,  
1038 A.C., Thorburn, P.J., Cammarano, D., Hatfield, J.L., Rosenzweig, C., Aggarwal, P.K.,  
1039 Angulo, C., Basso, B., Bertuzzi, P., Biernath, C., Brisson, N., Challinor, A.J., Doltra,  
1040 J., Gayler, S., Goldberg, R., Grant, R.F., Heng, L., Hooker, J., Hunt, L.A., Ingwersen,  
1041 J., Izaurralde, R.C., Kersebaum, K.C., Müller, C., Kumar, S.N., Nendel, C., O’leary,  
1042 G., Olesen, J.E., Osborne, T.M., Palosuo, T., Priesack, E., Ripoche, D., Semenov,  
1043 M.A., Shcherbak, I., Steduto, P., Stöckle, C.O., Stratonovitch, P., Streck, T., Supit, I.,  
1044 Tao, F., Travasso, M., Waha, K., White, J.W., Wolf, J., 2015. Multimodel ensembles  
1045 of wheat growth: many models are better than one. *Global Change Biology* 21, 911–  
1046 925. <https://doi.org/10.1111/gcb.12768>
- 1047 McMahon, T.A., Peel, M.C., Lowe, L., Srikanthan, R., McVicar, T.R., 2013. Estimating  
1048 actual, potential, reference crop and pan evaporation using standard meteorological  
1049 data: a pragmatic synthesis. *Hydrology and Earth System Sciences* 17, 1331–1363.  
1050 <https://doi.org/10.5194/hess-17-1331-2013>
- 1051 Medlyn, B.E., Dreyer, E., Ellsworth, D., Forstreuter, M., Harley, P.C., Kirschbaum, M.U.F.,  
1052 Le Roux, X., Montpied, P., Strassmeyer, J., Walcroft, A., Wang, K., Loustau, D.,  
1053 2002. Temperature response of parameters of a biochemically based model of  
1054 photosynthesis. II. A review of experimental data. *Plant, Cell & Environment* 25,  
1055 1167–1179. <https://doi.org/10.1046/j.1365-3040.2002.00891.x>
- 1056 Merganičová, K., Merganič, J., Lehtonen, A., Vacchiano, G., Sever, M.Z.O., Augustynczyk,  
1057 A.L.D., Grote, R., Kyselová, I., Mäkelä, A., Yousefpour, R., Krejza, J., Collalti, A.,  
1058 Reyer, C.P.O., 2019. Forest carbon allocation modelling under climate change. *Tree*  
1059 *Physiology* 39, 1937–1960. <https://doi.org/10.1093/treephys/tpz105>
- 1060 Olin, S., Schurgers, G., Lindeskog, M., Wårlind, D., Smith, B., Bodin, P., Holmér, J., Armeth,  
1061 A., 2015. Modelling the response of yields and tissue C : N to changes in atmospheric  
1062 CO<sub>2</sub> and N management in the main wheat regions of western Europe. *Biogeosciences*  
1063 12, 2489–2515. <https://doi.org/10.5194/bg-12-2489-2015>
- 1064 Parton, W.J., Holland, E., Del Grosso, S., Hartman, M., Martin, R., Mosier, A.R., Ojima, D.,  
1065 Schimel, D., 2001. Generalized model for NO<sub>x</sub> and N<sub>2</sub>O emissions from soils. *Journal*  
1066 *of Geophysical Research: Atmospheres* 106, 17403–17419.
- 1067 Pásztor, L., A. Laborczi, K. Takács, G. Illés, J. Szabó, and G. Szatmári. 2020. Progress in the  
1068 elaboration of GSM conform DSM products and their functional utilization in  
1069 Hungary. *Geoderma Regional* 21. ISSN 2352-0094,  
1070 <https://doi.org/10.1016/j.geodrs.2020.e00269>
- 1071 Peaucelle, M., Janssens, I., Stocker, B., Ferrando, A., Fu, Y., Molowny-Horas, R., Ciais, P.,  
1072 Penuelas, J., 2019. Spatial variance of spring phenology in temperate deciduous  
1073 forests is constrained by background climatic conditions. *Nature Communications* 10.  
1074 <https://doi.org/10.1038/s41467-019-13365-1>
- 1075 Rawls, J. , Onstad, W., A. Richardson, H., 1980. Residue and Tillage Effects on SCS Runoff  
1076 Curve Numbers. *Transactions of the ASAE* 23, 357–0361.  
1077 <https://doi.org/10.13031/2013.34585>
- 1078 Richardson, A.D., Keenan, T.F., Migliavacca, M., Ryu, Y., Sonnentag, O., Toomey, M.,  
1079 2013. Climate change, phenology, and phenological control of vegetation feedbacks to  
1080 the climate system. *Agricultural and Forest Meteorology* 169, 156–173.  
1081 <https://doi.org/10.1016/j.agrformet.2012.09.012>





- 1082 Ritchie, J.T., 1998. Soil water balance and plant water stress. in: Tsuji, G.Y., Hoogenboom,  
1083 G., Thornton, P.K. (Eds.): Understanding Options for Agricultural Production.  
1084 Springer Netherlands, Dordrecht, pp. 41–54. [https://doi.org/10.1007/978-94-017-](https://doi.org/10.1007/978-94-017-3624-4_3)  
1085 [3624-4\\_3](https://doi.org/10.1007/978-94-017-3624-4_3)
- 1086 Ritchie, J. T., 1981. Water dynamics in the soil-plant-atmosphere system. *Plant and Soil*, 58,  
1087 81-96. <https://doi.org/10.1007/BF02180050>
- 1088 Running, S., Hunt, E.R., 1993. Generalization of a Forest Ecosystem Process Model for Other  
1089 Biomes, BIOME-BGC, and an Application for Global-Scale Models.
- 1090 Running, S.W., Gower, S.T., 1991. FOREST-BGC, A general model of forest ecosystem  
1091 processes for regional applications. II. Dynamic carbon allocation and nitrogen  
1092 budgets1. *Tree Physiology* 9, 147–160. <https://doi.org/10.1093/treephys/9.1-2.147>
- 1093 Sándor, R., Barcza, Z., Acutis, M., Doro, L., Hidy, D., Köchy, M., Minet, J., Lellei-Kovács,  
1094 E., Ma, S., Perego, A., Rolinski, S., Ruget, F., Sanna, M., Seddaiu, G., Wu, L.,  
1095 Bellocchi, G., 2017. Multi-model simulation of soil temperature, soil water content  
1096 and biomass in Euro-Mediterranean grasslands: Uncertainties and ensemble  
1097 performance. *European Journal of Agronomy* 88, 22–40.  
1098 <https://doi.org/10.1016/j.eja.2016.06.006>
- 1099 Schwalm, C., Schaefer, K., Fisher, J., Huntzinger, D., Elshorbany, Y., Fang, Y., Hayes, D.,  
1100 Jafarov, E., Michalak, A., Piper, M., Stofferahn, E., Wang, K., Wei, Y., 2019.  
1101 Divergence in land surface modeling: Linking spread to structure. *Environmental*  
1102 *Research Communications* 1. <https://doi.org/10.1088/2515-7620/ab4a8a>
- 1103 Smith, N.G., Dukes, J.S., 2013. Plant respiration and photosynthesis in global-scale models:  
1104 incorporating acclimation to temperature and CO<sub>2</sub>. *Global Change Biology* 19, 45–63.  
1105 <https://doi.org/10.1111/j.1365-2486.2012.02797.x>
- 1106 Thomas, Q., Bonan, G., Goodale, C., 2013. Insights into mechanisms governing forest carbon  
1107 response to nitrogen deposition: A model–data comparison using observed responses  
1108 to nitrogen addition. *Biogeosciences* 10, 3869–3887. [https://doi.org/10.5194/bg-10-](https://doi.org/10.5194/bg-10-3869-2013)  
1109 [3869-2013](https://doi.org/10.5194/bg-10-3869-2013)
- 1110 Thornton, P.E., Rosenbloom, N.A., 2005. Ecosystem model spin-up: Estimating steady state  
1111 conditions in a coupled terrestrial carbon and nitrogen cycle model. *Ecological*  
1112 *Modelling* 189, 25–48. <https://doi.org/10.1016/j.ecolmodel.2005.04.008>
- 1113 Tillman, F.D., Weaver, J.W., 2006. Uncertainty from synergistic effects of multiple  
1114 parameters in the Johnson and Ettinger (1991) vapor intrusion model. *Atmospheric*  
1115 *Environment* 40, 4098–4112. <https://doi.org/10.1016/j.atmosenv.2006.03.011>
- 1116 USDA, 1987. [https://www.nrcs.usda.gov/Internet/FSE\\_DOCUMENTS/stelprdb1044818.pdf](https://www.nrcs.usda.gov/Internet/FSE_DOCUMENTS/stelprdb1044818.pdf)
- 1117 Verbeeck, H., Samson, R., Verdonck, F. and Lemeur, R., 2006. Parameter sensitivity and  
1118 uncertainty of the forest carbon flux model FORUG: a Monte Carlo analysis. *Tree*  
1119 *Physiology* 26, 807-817.
- 1120 Vetter, M., Churkina, G., Jung, M., Reichstein, M., Zaehle, S., Bondeau, A., Chen, Y., Ciais,  
1121 P., Feser, F., Geyer, R., Jones, C., Papale, D., Tenhunen, J., Tomelleri, E., Trusilova,  
1122 K., Viovy, N., Heimann, M., 2008. Analyzing the causes and spatial pattern of the  
1123 European 2003 carbon flux anomaly in Europe using seven models. *Biogeosciences*  
1124 *Discussions*, v.4, 1201-1240 (2007) 5. <https://doi.org/10.5194/bg-5-561-2008>
- 1125 Wallace, J.S., Holwill, C.J., 1997. Soil evaporation from tiger-bush in south-west Niger.  
1126 *Journal of Hydrology* 188–189, 426–442. [https://doi.org/10.1016/S0022-](https://doi.org/10.1016/S0022-1694(96)03185-X)  
1127 [1694\(96\)03185-X](https://doi.org/10.1016/S0022-1694(96)03185-X)
- 1128 White, M., Thornton, P., Running, S., Nemani, R., 2000. Parameterization and Sensitivity  
1129 Analysis of the BIOME–BGC Terrestrial Ecosystem Model: Net Primary Production  
1130 Controls. *Earth Interactions - EARTH INTERACT* 4. [https://doi.org/10.1175/1087-](https://doi.org/10.1175/1087-3562(2000)004<0003:PASAOT>2.0.CO;2)  
1131 [3562\(2000\)004<0003:PASAOT>2.0.CO;2](https://doi.org/10.1175/1087-3562(2000)004<0003:PASAOT>2.0.CO;2)



- 1132 Woodrow, I., Berry, J., 2003. Enzymatic Regulation of Photosynthetic CO<sub>2</sub> Fixation in C<sub>3</sub>  
1133 Plants. *Annual Review of Plant Physiology and Plant Molecular Biology* 39, 533–594.  
1134 <https://doi.org/10.1146/annurev.pp.39.060188.002533>  
1135 Zimmermann, M., Leifeld, J., Schmidt, M.W.I., Smith, P., Fuhrer, J., 2007. Measured soil  
1136 organic matter fractions can be related to pools in the RothC model. *European Journal*  
1137 *of Soil Science* 58, 658–667. <https://doi.org/10.1111/j.1365-2389.2006.00855.x>  
1138